Evaluation of Cre Recombinase Models for the Study of Dnmt3a Mutations and Myeloid Bias in Clonal Hematopoiesis

Evaluation of Cre Recombinase Models for the Study of Dnmt3a Mutations and Myeloid Bias in Clonal Hematopoiesis

Elizabeth Culpepper

A Thesis in the Field of Biology

for the Degree of Master of Liberal Arts in Extension Studies

Harvard University

May 2024

Abstract

The process of aging has been found to have lasting effects on hematopoietic stem cells and their ability to maintain the homeostasis of the hematopoietic system. From the accumulation of DNA damage to the biased differentiation potential toward myeloid lineages, the effects of HSC aging have been shown to disrupt normal HSC function and result in hematological malignancies and illness. Additional research on the repercussions of HSC aging must be conducted to fully understand its association with hematological disease and the mechanisms underlying this disease development. The current paper evaluates the efficacy of Cre recombinase models developed to examine the age-related myeloid bias and the frequent mutation of Dnmt3a associated with aged HSCs.

The first project investigated the ability of a Cre recombinase system to generate Dnmt3a R878H mutations in HSCs through the excision of the endogenous R878H exon 23 and the subsequent expression of fluorescent protein tdTomato. Due to a size difference in the respective regions controlling the expression of tdTomato and the wild-type R878H exon 23, exposure to Cre recombinase could result in the isolated expression of tdTomato without the coinciding expression of mutant Dnmt3a. Using FACS-facilitated single-cell isolation and expansion, HSCs were collected from TAM-treated experimental mice and genetically tested for the expression of both tdTomato and the Dnmt3a R878H mutation with PCR. Although Cre recombinase exposure was expected to result in the expression of the mutant Dnmt3a, primers detecting Dnmt3a wild-type and mutant exons were only able to generate bands corresponding to the wild-type exon

23 for the isolated HSC DNA. Similarly, primers specifically detecting the excision of the Dnmt3a wild-type were also unable to produce any bands. Overall, despite efforts to troubleshoot and optimize PCR performance, western blots examining the excision of the endogenous Dnmt3a exon were unable to generate sufficient results, suggesting an issue with the DNA isolation protocol or with the Dnmt3a excision primers themselves.

The second project examined a Cre recombinase system designed to simulate the myeloid dominance observed in older individuals through the depletion of multipotent progenitors. Embryonic multipotent progenitors have recently been identified as a significant but gradually decreasing source of lymphoid cells, implicating the cell type in the aged body's reduced presence of lymphoid cells and characteristic myeloid skew. Peripheral blood samples from experimental and control mice were examined using flow cytometry for potential changes to the myeloid and lymphoid cell types over a three-month period. In experimental samples, the CD4 T cell population was observed increasing upon the initial depletion of MPPs. However, this growth eventually resolved and experimental T cell counts lowered to those seen in controls. Similar results were also observed in the production of CD8 T cells. Additionally, experimental mice had generally high, unchanging CD19 B cell levels. All in all, more research is needed to further understand the changes observed in this project and the repercussions of MPP depletion on myeloid and lymphoid cells.

Dedication

I would like to give a special thanks to my parents, Christian and Toni Culpepper, for their continuous support throughout this research and thesis process. My personal and academic success thus far would not be possible without their countless sacrifices and unwavering love and support.

Acknowledgments

This thesis would not have been possible without the dedicated support and guidance of Dr. Fernando Camargo and Dr. Edward Quach. I would like to express my immense gratitude and appreciation for their mentorship, encouragement, and support in this project and my academic growth. I also want to thank the rest of the Camargo lab who were a great source of help and inspiration. Finally, the input of my thesis and research committee, Gail Dourian, Trudi Goldberg Pires, Dr. James Morris, and Joan Short, was also essential to this project and I hope to extend my warmest thanks.

Table of Contents

List of Figures

Chapter I.

Introduction

The establishment and maintenance of the blood system is essential for the preservation of human health. However, adverse health conditions such as infection and inflammation can cause the various cell types that constitute the hematopoietic system to become depleted. These cells include red blood cells, innate immune cells such as neutrophils and monocytes, and adaptive immune cells such as T cells and B cells (Luis et al. 2019). New blood cells must be constantly produced to maintain homeostasis and support the body's immune response. Hematopoietic stem cells, or HSCs, are responsible for this continuous replenishment of mature, adult blood cells.

HSCs and the Hematopoietic System

Residing in small numbers in the bone marrow niche, HSCs have historically been considered to be the only cells within the hematopoietic system that possess the potential for both multi-potency and self-renewal. Multipotency refers to an HSC's ability to differentiate into all of the functional blood cells that encompass the blood system (Seita and Weissman 2010). From this, the proposed HSC lineage tree is established, in which HSCs act as the leader of a hierarchy of progenitors that become progressively restricted to several or single lineages (fig. 1). These blood progenitors eventually expand to produce more mature blood precursors devoted to uni-lineage differentiation and the production of mature blood cells. In addition to multipotency, HSCs also have the ability of self-renewing. Self-renewal is defined as the ability to give

rise to identical daughter HSCs without differentiation, enabling the maintenance of HSC pool size and their continued production of differentiated progenitors (Orkin and Zon 2008). Because of this, the regulation of both self-renewal and multipotency is essential to supporting hematopoietic homeostasis. However, certain physiological conditions such as stress or aging have been shown to disrupt this stability and result in detrimental repercussions (Orkin and Zon 2008). Understanding the mechanisms underlying HSC homeostasis and its potential deregulation is imperative to understanding the pathogenesis of hematological malignancies.

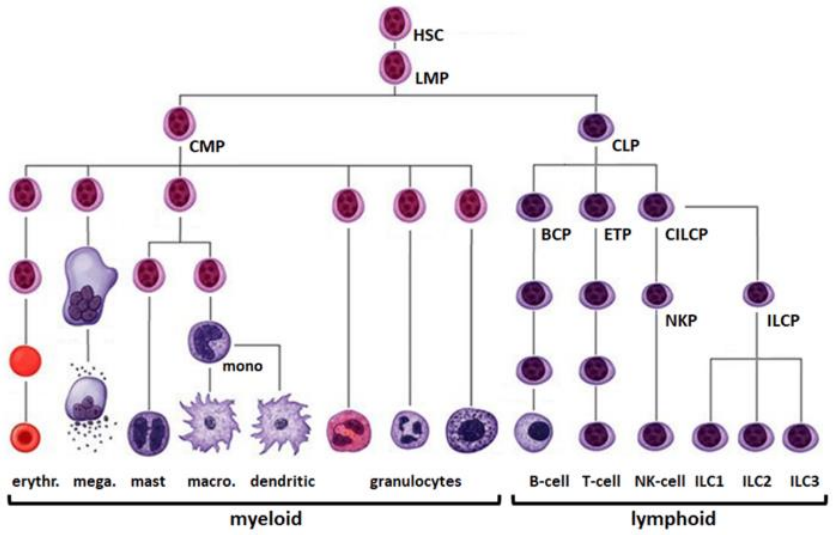

Figure 1. Hematopoietic Stem Cell Lineages.

Fig. 1 demonstrates the hierarchy of blood progenitors, in which multipotential hematopoietic stem cells sit at the top and eventually differentiate into either common myeloid or lymphoid progenitors. From myeloid progenitors come megakaryocytes, erythrocytes, mast cells, and myeloblasts. Megakaryocytes will later develop into thrombocytes whereas myeloblasts will later develop into basophils, neutrophils, eosinophils, and monocytes which differentiate into macrophages. Common lymphoid progenitors, on the other hand, differentiate into natural killer cells and T cells and B cells. Reprinted from Nagel, Stephen. "NKL-Code in Normal and Aberrant

Hematopoiesis." Cancers, vol. 13, no. 8, 2021, https://doi.org/10.3390/cancers13081961. Accessed 7 September 2023.

The Effects of Aging on HSCs

The incidence of hematological disease progressively increases with age, to the point that aging itself has been identified as a leading risk factor for cardiovascular disease. In the human blood system, for instance, aging has been found to induce extracellular factors that lead to alterations in cellular function. Specifically, HSC aging is associated with increased HSC numbers, cellular exhaustion inflammation, reduced self-renewal capacity, limited reconstitution, and diminished protein quality control (fig. 2). With age, HSCs produce increased numbers of functionally impaired HSCs with reduced self-renewal and decreased protein control (Bousounis et al. 2021). Furthermore, the aging of HSCs has also been found to result in myeloid bias, DNA damage and epigenetic changes and clonal hematopoiesis.

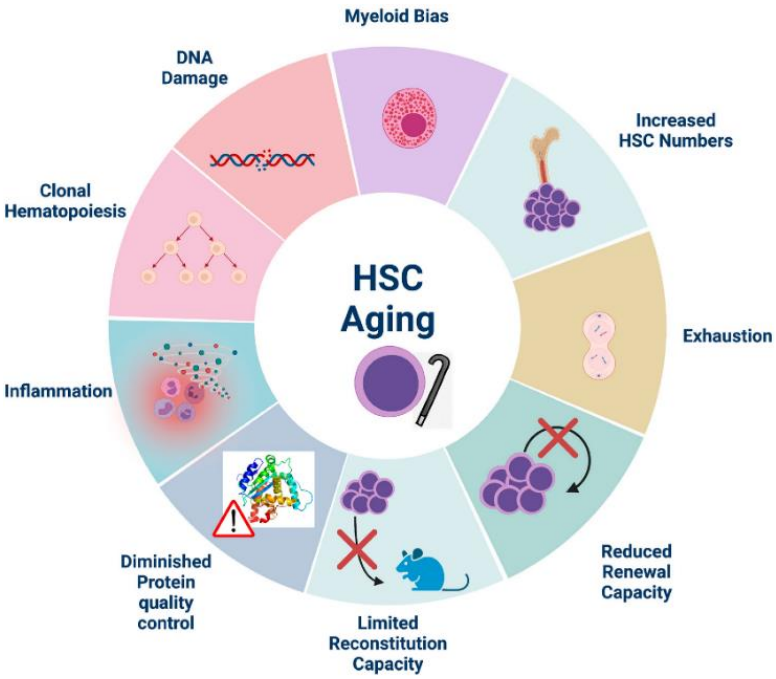

Figure 2. HSC Aging.

Fig. 2 shows the repercussions of HSC aging including: DNA damage, myeloid bias, inflammation, exhaustion, clonal hematopoiesis, increased HSC numbers, reduced renewal capacity, limited reconstitution capacity, and diminished protein quality control. Retrieved from Bousounis, Pavlos, et al. "Inflammation and HSC Aging." Cell, vol. 10, no. 6, 2021, https://doi.org/10.3390/cells10061386. Accessed 7 September 2023.

Under normal, steady-state conditions, HSCs differentiate into balanced myeloid and lymphoid lineages (fig. 1). Aged HSCs, on the other hand, exhibit abnormal differentiation which is characterized by an increased differentiation potential to the myeloid lineage and a decreased contribution to the lymphoid lineage, resulting in a myeloid progenitor bias (Meija-Ramirez and Florian 2020). This is important because aged adults are more likely to have compromised adaptive immunity and experience a higher prevalence of anemia (Lee et al. 2019). Lymphoid cells notably differentiate into T cells and B cells, which are fundamental to the body's immune system. Therefore, a

decrease in lymphoid progenitors could account for the elderly's well-established predisposition to illness and infection (Gardner 1980; Kline and Bowdish 2016; Guo et al. 2022). Further research into the cause of myeloid bias could provide valuable insights into age-related susceptibility to illness.

In addition to myeloid bias, the accumulation of DNA damage is also a frequent outcome of aging among HSCs and has been shown to result in age-related hematological malignancies and degeneration. Although HSCs have protective mechanisms that safeguard their genome from DNA alterations, some specific mutations are known to be particularly persistent among HSCs, including mutations among the epigenetic regulators Dnmt3a, Tet2, and Asxl1 (Jaiswal and Ebert 2019). Throughout aging, these somatic mutations expand within the aged HSC population until these mutant HSCs become the most prevalent contributors to the hematopoietic system (Luis et al. 2019). Furthermore, these mutations regularly appear over-expressed in healthy, older individuals and patients with blood malignancies such as myelodysplastic syndrome and acute myeloid leukemia (Meija-Ramirez and Florian 2020). Thus, these mutations are significantly associated with aging and competitive advantages that lead to over-expression within the blood cell pool, eventually leading to clonal hematopoiesis.

Age-related clonal hematopoiesis, or ARCH, is defined as the gradual expansion of HSCs carrying disruptive and recurrent genetic variants. As briefly mentioned before, this process is a consequence of the accumulation of HSC mutations during aging. In normal conditions, hematopoiesis is supported by different HSCs with similar differentiation potential. However, in the case of ARCH, specific mutated HSC clones disproportionately contribute to the peripheral blood population. While this may seem

like a minor occurrence, ARCH is associated with many age-related physiological conditions, including inflammation, vascular diseases, cancer mortality, and elevated risk for acute myeloid leukemia, or AML (Shulsh 2018). It is important to note that ARCH is only a risk factor for acute myeloid leukemia, and only 10% of clonal hematopoiesis cases progress to AML (Luis et al. 2019). However, the factors that determine whether ARCH advances into hematological disease are not currently known and it is imperative that more research is conducted to develop potential therapies that could suppress this progression of ARCH into illness.

This research project is centered around how age-related clonal hematopoiesis influences the various populations of blood progenitors, specifically through the frequent mutation of DNMT3A and age-associated myeloid dominance.

Chapter II.

Introduction

The first project examined a Cre recombinase model that was developed to examine the frequent mutation of Dnmt3a in aged HSCs.

Dnmt3a Mutant and tdTomato

Adult malignancies are thought to arise through the gradual accumulation of oncogenic mutations within HSCs. Notably, HSCs are estimated to develop ~20 somatic mutations per year (Jaiswal 2020), which persist for the lifetime of an individual due to HSCs being a long-lived cell-type with the capacity for self-renewal. Considering that the average person has over 50,000 HSCs, it is estimated that one could acquire over 350,000 coding mutations within the HSC pool by 70 years of age (Jaiswal and Ebert 2019). Although most of these mutations will likely be neutral, a mutation driving either a selective advantage or disadvantage of an HSC clone will be disproportionately represented. Using large datasets from high-throughput targeted sequencing methodologies, researchers have identified three genes that experience persistent mutations that increase in frequency with age, reaching 10-20% of the clonal contribution in older individuals (McKerrell et al. 2015; Genovese et al. 2014; Jaiswal et al. 2014). One of these genes that was determined to be a frequent site of mutation was DNMT3A, or DNA methyltransferase 3A.

The Dnmt3a Protein

Belonging to a family of highly conserved DNA methyltransferases that catalyze 5-methylcytosine methylation, DNMT3A is a 130kDA protein encoded by 23 exons on human chromosome 2p23 (Yang et al. 2015). DNMT3A is made up of a catalytic region, which is responsible for catalyzing 5-cytosine methylation within CpG dinucleotides, and a regulatory region, which promotes nuclear localization of the enzyme, chromatin targeting, and interactions with allosteric regulators (Venugopal et al. 2021). The regulatory region consists of the N-terminal, the Pro-Trp-Trp-PRO (PWWP) domain, and the ATRX-DNMT3-DNMT3L (ADD) domain (fig. 3A). The PWWP domain is required for targeting to tri- and dimethylate H3K36 marking gene bodies, whereas the ADD domain binds to unmethylated H3K3 that marks inactive chromatin. Overall, the domains of DNMT3A are highly conserved in vertebrates with 98% homology between humans and mice (Xie et al. 1999). However, impairment of DNMT3A domain function and domain-domain interactions can arise with the frequent occurrence of mutations throughout the protein.

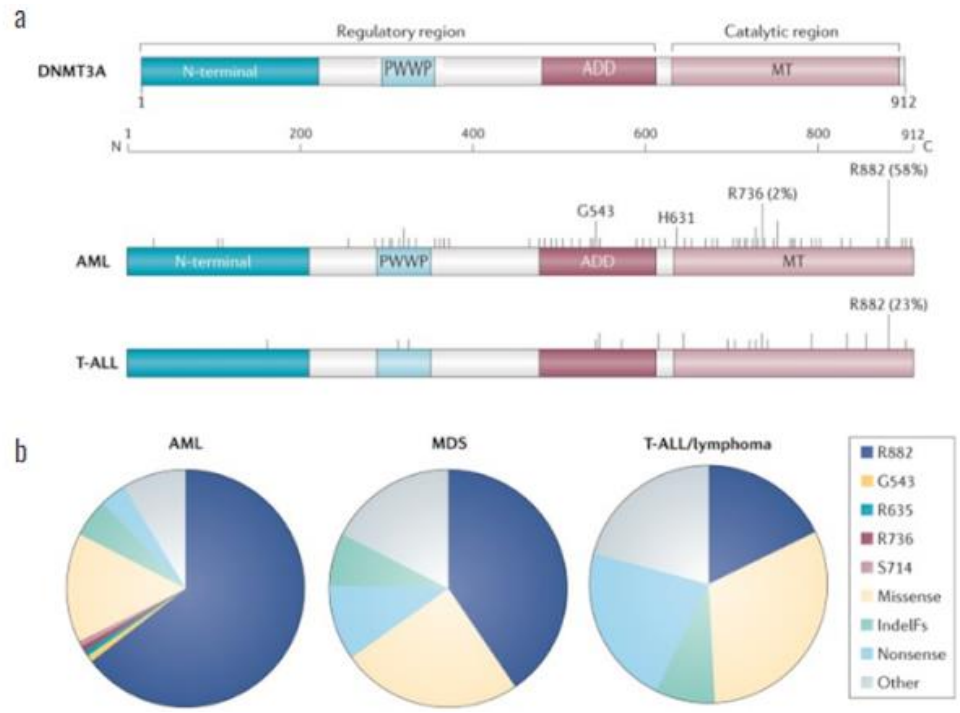

Figure 3. Structure of Dnmt3a and Common Sites of Mutation.

Fig. 3 depicts DNA methyltransferase 3a and hotspot mutations that are prevalent amongst cases of AML and T-ALL. Fig. 3A illustrates the functional domains that make up Dnmt3a, including the N-terminal, the PWWP, and the ADD, and the catalytic region. Fig. 3B shows the location of Dnmt3a mutations, with the top band indicating amino acid position and scale. The vertical lines represent the mutations mapped to Dnmt3a in acute myeloid leukemia and T cell lymphoblastic leukemia in a subset of patients in which the entire gene was sequenced. The frequent mutation at R882 in AML versus T-ALL is also illustrated, with minor hotspots in AML also indicated. Fig. 3C demonstrates the frequency of mutations in AML, myelodysplastic syndrome, and T-ALL/lymphoma, sourced from the Catalog of Somatic Mutations in Cancer database. In both AML and myelodysplastic syndrome, the majority of mutations are at R882, but only account for a fraction of T-ALL/lymphoma mutations. Retrieved from Yang, Liubin, et al. "DNMT3A in haematological malignancies." Nature Reviews Cancer, vol. 15, no. 3, 2015, pp. 152-165, https://doi.org/10.1038%2Fnrc3895. Accessed 10 October 2023.

Frequent Mutation of Dnmt3a

Since the discovery of its recurrent mutations in acute myeloid leukemia, DNMT3A has become well-established as one of the most frequently mutated genes in a

variety of hematological malignancies and has been found to play a significant role in clonal and malignant hematopoiesis. Although some mutations have been reported in other members of the DNA methyltransferase family including DNMT1 and DNMT3B, there is an overwhelming presence of DNMT3A mutations across a range of diseases. For example, during cancer development, DNMT3A mutations in HSCs occur early-on and form pre-leukemic lesions, acting as an indicator for poor prognosis in acute myeloid leukemia (Brunetti et al. 2017). Additionally, both myeloid and lymphoid malignancies are significantly associated with DNMT3A mutations (Yang et al. 2015). Although the domains of DNMT3A that are enriched for mutations vary between malignancies, one residue has particularly distinguished itself as a mutational hotspot: arginine 882.

Arginine 882, or R882, is located in the methyltransferase domain at exon 23 of DNMT3A and is frequently mutated in a multitude of diseases, with a significant presence specifically in acute myeloid leukemia. Within the 25% of AML cases that report DNMT3A mutations, around 60% report mutations at residue R882 (fig. 3B). Across other myeloid malignancies such as myelodysplastic syndrome and chronic myelomonocytic leukemia, R882 is also frequently mutated, though to a lesser extent than in AML. Comparatively, mutations in myeloid malignancies largely reside on R882, whereas lymphoid lineage malignancies have mutations that are distributed throughout the domain region. Despite this, there are still a considerable number of R882 mutations in lymphoid malignancies. As figure 3A demonstrates, in T cell lymphoblastic leukemia, R882 mutations account for 23% of DNMT3A mutations in patients. Additionally, in regard to variant characteristics, R882 mutations are typically heterozygous, with biallelic involvement largely restricted to the more marginal number of non-R882 mutations. For

R882 mutations, some Dnmt3a wild-type function seems to remain in the heterozygous state, whereas heterozygous mutations at other sites may lower activity of the wild-type protein to a point insufficient to drive malignancy (Yang et al. 2015). Overall, the overwhelming prevalence of DNMT3A mutations found at R882 has made the residue a subject of substantial research and investigation, but there is still much to be understood about the residue.

Chapter III.

Methods

This project examined the efficiency of an inducible CreER-loxP recombinase system that was developed to investigate the R878 mutation, which replicates the human R882 mutation, in mice.

Dnmt3a Mutant and tdTomato

Previously, Dnmt3afl-R878H mice were designed to conditionally express the mutant protein DNMT3A R878H after administration of the selective estrogen receptor modulator Tamoxifen and subsequent exposure to Cre recombinase (Loberg et al. 2019). The Dnmt3afl-R878H construct design consisted of a loxP-flanked Dnmt3a exon 23 and polyA STOP sequence, followed by a modified Dnmt3a exon 23 sequence encoding for the R878H mutation (fig. 4). Endogenous Dnmt3a is expressed under normal conditions and when exposed to Cre, the loxP-flanked endogenous exon 23 is deleted and replaced with the R878H mutant exon, resulting in expression of the Dnmt3a mutant. While the present targeting strategy builds upon the previously described Dnmt3afl-R878H model, our design has unique benefits to examining the mutant Dnmt3a phenotype. It remains time sensitive due to the Tamoxifen-dependent inducible CreER recombinase, but also features tissue specificity as the cassette is located in the HSC-specific Fgd5 promoter region (Gazit et al. 2014). Additionally, the current construct design not only includes the conditional expression of mutant Dnmt3a, but also of the red fluorescent protein variant tdTomato. When mice are treated with Tamoxifen (TAM), CreER is activated and excises a loxP-flanked stop sequence located in the Rosa26 locus, resulting in the

transcription of tdTomato. At the same time, CreER should also excise the loxP-flanked endogenous exon 23 in the Dnmt3a locus, enabling the expression of the monoallelic R878H mutation. However, the lox-STOP-lox sequence is a much smaller area to excise than the wild-type exon region. Because of this, CreER could potentially only excise the LSL area, leading to Tomato being expressed but not the mutant Dnmt3a. This would mean that when these mice are used in later experiments, the effects of mutant Dnmt3a in HSCs would not actually be observed. Therefore, this experiment is important because it would demonstrate the efficacy of the Cre recombinase system, characterized by the successful targeting of the endogenous exon 23, the subsequent expression of the R878H mutant exon, and the coinciding expression of tdTomato.

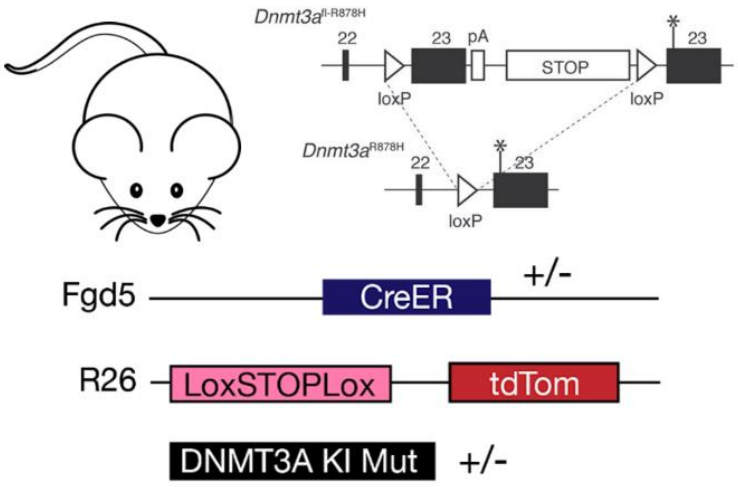

Figure 4. Fgd5CreER-Lox System.

Fig. 4 illustrates how the Fgd5CreER-Lox system works. In the Rosa loci, there is a lox-STOP-lox locus, the lox is indicated by the triangles and the stop is indicated by the STOP text box. In the Dnmt3a loci, the wild-type exon 23 is surrounded by loxP, with both a poly-A tail (indicated by the pA) and a STOP sequence. Under normal transcription, the endogenous Dnmt3a will be expressed as the polyA STOP sequence

results in transcription termination. However, when treated with Tamoxifen, CreER will excise both the STOP locus and the wild-type exon 23, allowing the transcription of tdTomato and the mutant R878H. This will result in the expression of mutant Dnmt3a in HSCs and allow them, and their subsequent progeny, to be fluorescently labeled as red. Created using BioRender.com, accessed 10 October 2023.

To examine this relationship, Tomato+ long-term HSCs (LT-HSCs) were collected from all four limbs of TAM-injected Fgd5CreER|Tom/-|Dnmt3a+/- mice. Because HSCs account for only 0.01% of total nucleated cells in the bone marrow (Challen et al. 2009), obtaining bone marrow cells from all four limbs maximized the number of HSCs collected in a sample. Moreover, RBC lysis and enrichment of cKit-expressing cells by magnetic-activated cell sorting (MACS) allowed for further HSC optimization by narrowing down the cell populations present in a sample. Using fluorescently labeled antibodies for surface markers specific for LT-HSCs, the Tomato+ LT-HSCs were isolated and individually sorted into 96-well, round bottom cell culture plates using fluorescence-activated cell sorting, or FACS (fig. 5). Using FACS to isolate HSCs from bone marrow is a well-established technique that uses the negative selection of various lineage-specific markers and the positive selection for stem cell-specific surface markers: Sca-1 and c-Kit (Tian and Zhang 2016). Lineage markers included Ter119 for identification of erythrocytes, CR1 for granulocytes, B220 and CD19 for B cells, and CD3 for T cells. Next, the identification of the LT-HSC subtype was established with the expression of CD150 and absence of CD48. Therefore, the FACS gating for the isolation of the LT-HSC subtype was defined as Lineage -, Sca-1 +, c-Kit +, CD150 +, and CD48 -. Additionally, sorting these individual LT-HSCs into singular wells was important as it ensured that after expansion, all cells in a well would have the same genotype as they were all derived from the same original cell. As these original

cells were already established as Tomato+ from FACS, all of their subsequent progeny would also be Tomato+, which was later confirmed under a fluorescent microscope. Similarly, if the original cell was a Dnmt3a mutant, its daughter cells would also be Dnmt3a mutants. Therefore, allowing a single cell to expand after three weeks guaranteed that there would be enough cells of an identical genotype to isolate DNA from and run PCR for mutant Dnmt3a. This would allow me to determine the likelihood of a Tomato+ LT-HSC also being a Dnmt3a mutant and to demonstrate the overall efficacy of the CreER-LoxP recombinase system.

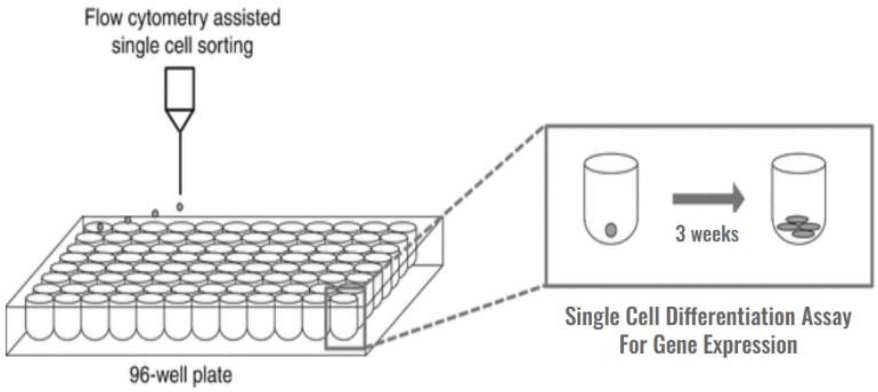

Figure 5. Single Cell Differentiation Assay.

Fig. 5 illustrates the single-cell expansion of LT-HSCs. Single-cell LT-HSCs are sorted individually into 96-well plates via fluorescence-activated cell sorting. These cells are allowed to expand for three weeks at which point they reach confluency and can be harvested to assess gene expression levels. Figure modified from Rhodes, Steven D., and Yang, Feng-Chun. "Single Cell Assay, Mesenchymal Stem Cells." Encyclopedia of Systems Biology, 2013, pp. 1947-1950, https://doi.org/10.1007/978-1-4419-9863-7_625. Accessed 10 October 2023.

Mouse Models

Fgd5CreER|Tom/-|Dnmt3a+/- mice were crossed and genotyped using PCR-based assays with tail DNA samples, prior to starting the experiment. Cre activation was induced by 40 mg intraperitoneal injection of TAM.

LT-HSC Collection

Total BM cells were isolated from all four limbs dissected from TAM-injected Fgd5CreER|Tom/-|Dnmt3a+/- mice, which were crushed using a mortar and pestle in PBS. After removal of red blood cells with RBC lysis buffer for 15 minutes, the cell suspension was filtered through a 70-um strainer to obtain a single-cell suspension and remove debris. Antibody staining using cKit+ MACS magnetic beads was performed for 30 minutes, followed by filtration with a 40-um strainer and subsequent magnetic column depletion. Cells were then stained with fluorescent monoclonal antibodies corresponding to the previously described LT-HSC phenotype (Lineage -, Sca-1 +, c-Kit +, CD48 -, CD150 +) for 40 minutes. Cell sorting was performed using a FACS Aria instrument. Single-color and no-color controls with non-enriched cells were used to ensure correct voltage and compensation setup. Data was analyzed with FlowJo software.

HSC Expansion Culture

Individual Tomato+ LT-HSCs isolated from Fgd5CreER|Tom/-|Dnmt3a+/- mice were cultured in 96-well, round bottom plates that had been manually coated with Fibronectin for one hour. Cell culture media consisted of F12 nutrient medium supplemented with 100 ng/mL ITS-X, 100 ng/mL HEPES buffer solution, 100 ng/mL L-glutamine, 100 ng/mL Penicillin/Streptomycin, 100 ng/mL TPO, 10 ng/mL SCF, and 91

ng/mL PVA. The latter three components have previously been shown to optimize HSC expansion (Wilkinson et al. 2019). After cells were initially plated, they were allowed to expand for five days before changing the media. At which point, half of the media was routinely replaced with fresh media twice a week for the three weeks that the cells were cultured. Cells were incubated at 37℃ in 5% CO2.

Dnmt3a Detection

DNA was isolated from cultured HSCs using a tail lysis buffer. With this isolated, genomic DNA, PCRs were performed using primers to detect Cre and CreER, tdTomato, and wild-type and mutant Dnmt3a. In addition to these, a primer that specifically detected the excision of the Dnmt3a wild-type exon 23 was also used. This Dnmt3a excision primer was made up of two forward primers and one shared reverse primer. From 5' to 3', the sequence of the first forward primer was CCACTAGAACCCTCAGCACA and the sequence for the second was AGTAAGTCTGCAGGTCGAGG. The reverse primer's sequence was CCCCAGACCTTTGAAATGCC. Gene expression levels were compared against those seen in control samples using tail DNA samples from B6 and Dnmt3a wild-type mice.

Chapter IV.

Results

Utilizing the previously described protocols for fluorescence-activated cell sorting, single cell HSC expansion, and the detection of mutant Dnmt3a using PCR, the following results were generated.

Dnmt3a Mutant and tdTomato

In order to determine the likelihood of a LT-HSC expressing both tdTomato and the Dnmt3a mutant exon 23, this project first investigated the Tomato+ LT-HSCs themselves before examining their expression of Dnmt3a.

Tomato+ Optimization

As explained previously, HSCs are a relatively rare cell type in the bone marrow and collecting all limbs from a mouse maximized the number of LT-HSCs collected in a sample. While that is an efficient way to ensure that there are more LT-HSCs in a sample, this experiment specifically used Tomato+ LT-HSCs. Therefore, it was also important to ensure an appropriate level of Tomato positivity among the LT-HSCs, otherwise the number of cells that could be sorted would have been severely restricted. Because the expression of tdTomato was dependent on Tamoxifen administration, determining the number of times TAM needed to be injected and how long post-injection to sac the mouse was essential. The regimen that generated the most significant amount of Tomato+ LT-HSCs involved a triple-injection of 1 mL of 40 mg Tamoxifen, with a week wait

period between each injection and the last injection occurring the day before sacrificing the mouse. The result of this approach is shown in figure 6.

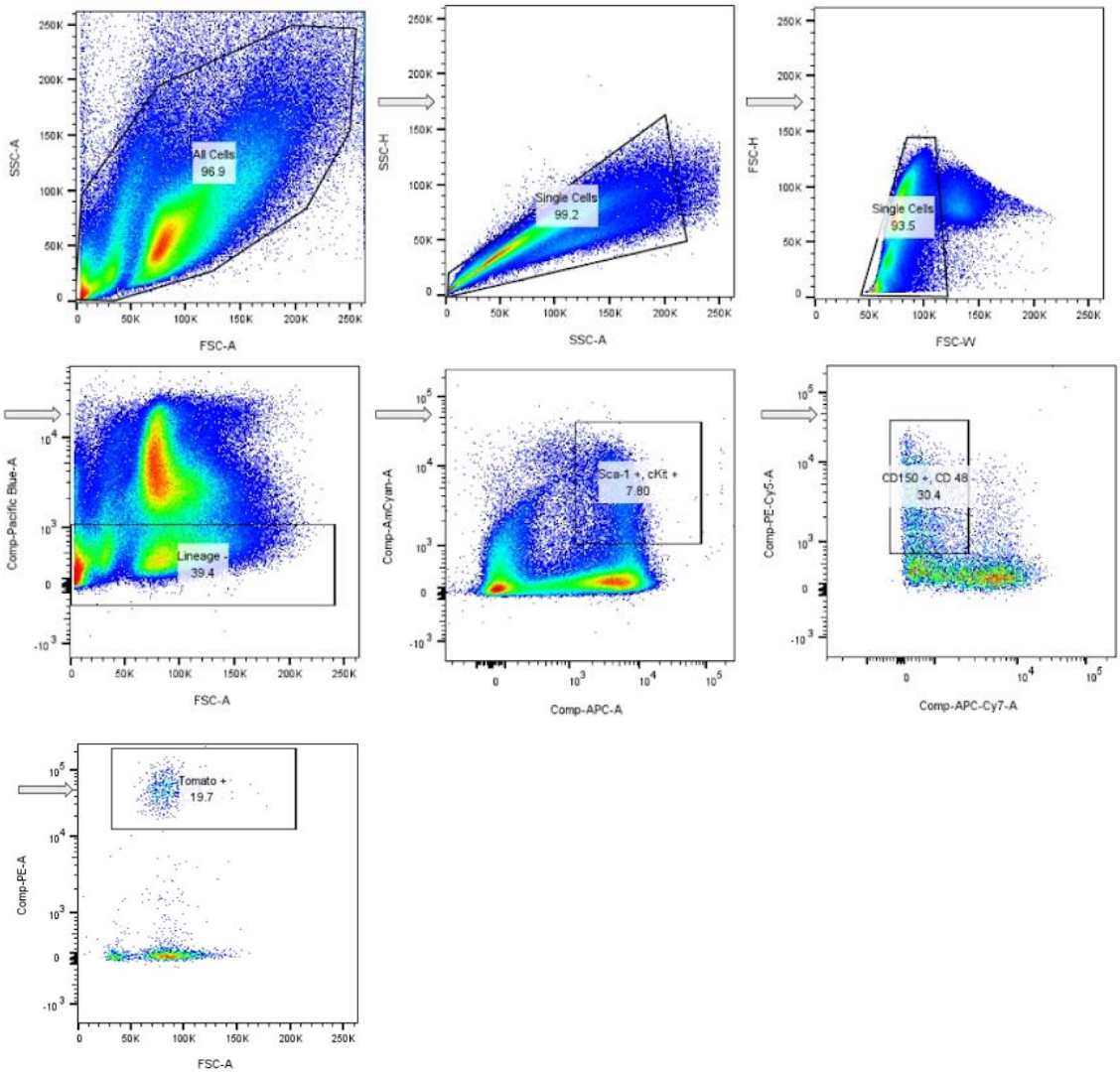

Figure 6. Single Cell Sort Data.

Fig. 6 demonstrates the gating strategy of Tomato+ LT-HSCs using fluorescence-activated cell sorting. Cells were first gated based on their forward (FSC-A) and side scattering (SSC-A). Doublets were then excluded, using side scatter height (SSC-H) versus side scatter area (SSC-A) and forward scatter height (FSC-H) versus forward scatter width (FSC-W). From this, the general HSC population was identified by

excluding cells expressing lineage-specific markers (Lineage -) and focusing on cells expressing stem cell-specific surface markers (Sca-1 +, c-Kit +). The long-term HSC subtype was then selected using the negative selection of CD48-expressing cells and the positive selection of CD150-expressing cells (CD150 +, CD48 -).

As one can see, there is a distinct Tomato positive population among the LT-HSCs (fig. 6). In samples from mice that had been administered using other Tamoxifen regimens, the Tomato+ LT-HSC population was not as segregated. Additionally, other Tamoxifen injection protocols did not yield as many Tomato+ LT-HSCs, whereas this regimen was able to fill several (~ 4) 98-well cell culture plates.

HSC Expansion

Tomato+ LT-HSCs were then individually sorted into Fibronectin-coated, 96-well plates that had been filled with cell culture media. While it was difficult to identify cells immediately after sorting using light microscopy, small visible clusters of cells usually emerged by 7 days post-sort. Cells were allowed to expand to confluency, which was reached at three weeks. At which point, the cells were harvested for DNA isolation. The fluorescence of all wells was verified before harvesting. Figure 7 shows a representative image of the typical well density and morphology at confluency.

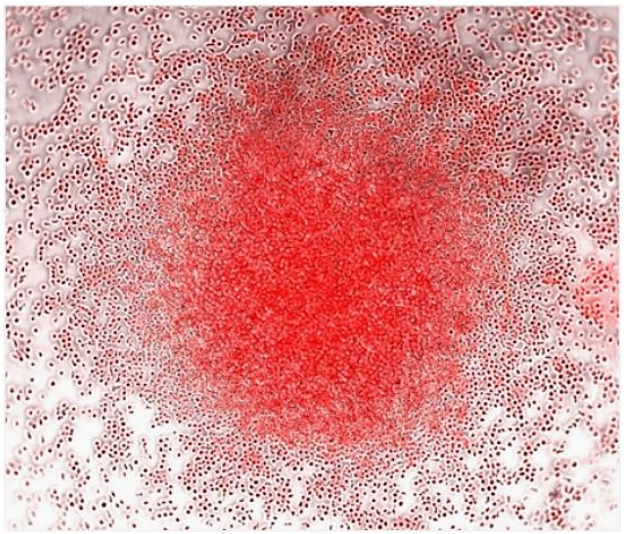

Figure 7. Cultured Tomato+ LT-HSCs.

Fig. 7 shows the expansion of the individually sorted Tomato+ LT-HSCs after 3 weeks. The majority of cells settle at the bottom of the well, with some expanding onto the walls. Furthermore, the morphology of the cells tends to be small and round, but larger cells can also be observed which are considered 'megakaryocyte-like.' Finally, all cells are exhibiting fluorescent ability, confirming that the original sorted cell was Tomato+. Images were taken at 5x magnification.

Dnmt3a Detection

DNA isolated from cultured HSCs was first examined with PCR using primers that detected CreER, tdTomato, and mutant and/or endogenous Dnmt3a. As demonstrated in figure 8, bands were obtained for Cre, CreER, and Tomato mutant primers. This was expected as the Fgd5CreER|Tom/-|Dnmt3a+/- mice that were used to obtain the LT-HSCs were genotyped beforehand and all cultured HSCs were able to be fluorescently imaged, which would only occur if CreER and tdTomato were both present. However, the Dnmt3a primers were only able to produce a single band. The Dnmt3a primers consisted of one shared forward primer and two reverse primers, one that was specific to

the wild-type exon and the other to the mutant exon. For samples that only have endogenous Dnmt3a present, a single band that corresponds to the wild-type exon should be produced. For uninduced samples that have the Dnmt3a mutant present in the Cre recombinase system, on the other hand, two bands should be produced – one that correlates to the wild-type exon and one to the mutant exon. Therefore, induced samples with the Fgd5CreER|Tom/-|Dnmt3a+/- genotype should have generated bands for only the mutant exon, as the wild-type exon 23 should have been excised out. This is important because despite genotyping the experimental mice for the Fgd5CreER|Tom/-|Dnmt3a+/- genotype prior to TAM administration, the induced mouse-derived, cultured HSCs were only able to produce the bottom wild-type exon band.

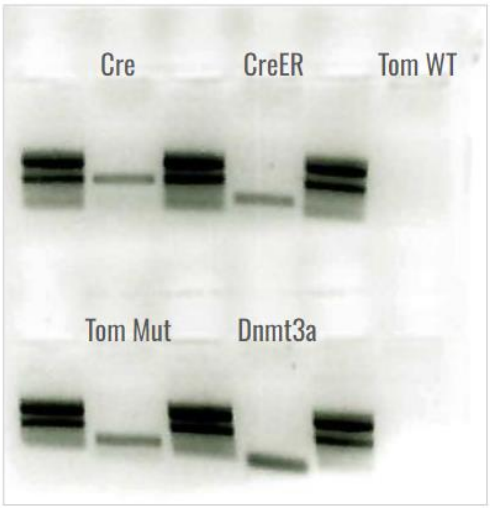

Figure 8. Dnmt3a Mutant Western Blot.

Fig. 8 displays the initial western blot analysis performed to detect Cre, CreER, Tomato wild-type (Tom WT), Tomato mutant (Tom Mut), and mutant or wild-type Dnmt3a in DNA isolated from cultured HSCs. Both Cre and CreER were identified, as well as Tomato mutant. Dnmt3a primers were only able to produce a single band, which corresponded to the wild-type exon.

One possible explanation for this was that the endogenous exon was in fact excised and the primers were mistakenly recognizing the mutant exon as the wild type. With the exception of the R878H mutation, the wild-type and mutant exons are otherwise indistinguishable from one another. Because of this, the correct identification of the Dnmt3a gene as a wild-type or mutant is dependent on the location of the primer markers within the locus. Specifically, in the absence of the endogenous exon, a primer detecting the wild-type exon could potentially generate a band, if the primer marker for the mutant exon was positioned before the R878H mutation. Therefore, primers that had been designed to specifically detect the excision of the Dnmt3a endogenous exon 23 were utilized.

Using the Dnmt3a excision primers, a subsequent western blot was performed on the isolated HSC DNA (fig. 9). In regard to samples that have the wild-type exon present, the Dnmt3a excision primers should generate a single band. For induced samples that have properly excised the wild-type exon and are expressing the mutant exon, the primers should produce two bands. In addition to the excision primers, the original Dnmt3a wild-type and mutant primers were also used. As a control, two tail DNA samples were examined, in addition to the cultured HSC DNA. One of the tails came from an uninduced mouse with the Dnmt3a+/- genotype, generating bands both with the Dnmt3a wild-type primer and the mutant primer, as expected. The second tail came from a mouse with the normal, wild-type Dnmt3a genotype and produced a band only for the Dnmt3a wild-type primer, which was also anticipated. Consistent with the results in figure 8, the cultured HSCs all showed bands with the Dnmt3a wild-type primer, but not with the Dnmt3a mutant primer. While it may seem like bands were produced with the Dnmt3a

mutant primers in the cultured HSCs (fig. 9), these bands are not located at the same bp as those generated from the Dnmt3a+/- tail sample. Because of this, it can be assumed that these are not actual bands that correlate to the presence of the Dnmt3a mutant exon and are likely the result of 'primer dimer'. Furthermore, for the Dnmt3a excision primer, bands were not able to be produced for any of the tail samples or the cultured HSCs, and primer dimer was also created. The tail samples should not have generated any bands for the Dnmt3a excision primer as the Dnmt3a wild-type tail did not have the Cre recombination system to begin with and the Dnmt3a+/- tail came from an uninduced mouse and therefore the Dnmt3a wild-type exon could not have been excised. However, because the LT-HSCs were derived from Tamoxifen-treated Fgd5CreER|Tom/-|Dnmt3a+/- mice, the samples should have produced bars if the wild-type exon had been excised.

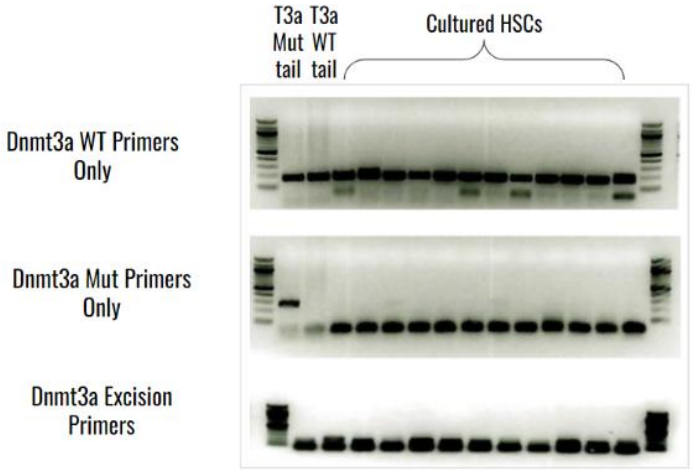

Figure 9. Dnmt3a Excision Western Blot.

Fig. 9 depicts the results of a western blot detecting the excision of Dnmt3a on DNA from the cultured HSCs. Following a 100 bp DNA ladder, the next two lanes are from mouse

tail DNA samples. The first tail was from a mouse with the Dnmt3a+/- genotype, whereas the second tail was from on with just the endogenous Dnmt3a. The Dnmt3a+/- tail sample generated bands both for the Dnmt3a wild-type primer and the Dnmt3a mutant primer, whereas the normal tail sample only produced a band for the Dnmt3a wild-type primer. The next lanes are all from isolated DNA from the cultured LT-HSCs. These samples were examined using primers that only detected the Dnmt3a wild-type exon, that only detected the Dnmt3a mutant exon, and that detected the excision of the Dnmt3a wild-type exon.

Chapter V.

Discussion

The western blots examining the expression of the Dnmt3a mutant exon and the excision of the Dnmt3a wild-type exon suggest several things.

Dnmt3a Mutant and tdTomato

There were many possible explanations as to why the cultured HSCs did not produce a band for the Dnmt3a excision primer, including an insufficient amount of DNA being loaded into the sample and problems with the PCR. Because of this, it was important to troubleshoot the PCR technique and perform subsequent western blots with PCRs of varied conditions, using DNA samples for the other 200 samples of cultured HSCs. PCRs were executed, in which the annealing temperature, the number of PCR cycles, and the amount of DNA input were all altered. All in all, these adjustments were futile as western blot analysis still produced either no bands or primer dimer. This suggests that there was a problem with the DNA isolation of the cultured HSCs or with the Dnmt3a excision primers themselves.

Chapter VI.

Introduction

The second project evaluated a Cre recombinase system designed to examine the age-related myeloid bias associated with HSCs.

MPPs and Myeloid Bias

The adult hematopoietic system is supported by the extensive self-renewal capacity and multilineage differentiation potential of HSCs. Despite the cell's importance, their contributions during embryonic development have not been able to be thoroughly investigated until recently due to difficulties with overlapping marker expression with other blood progenitors. During embryogenesis, hemogenic endothelial cells transform into hematopoietic cells, including lympho-myeloid progenitors, hematopoietic stem and progenitor cells, and erythron-myeloid progenitors (EMPs), through a process referred to as the endothelial-to-hematopoietic transition, or EHT. EMPs then leave the yolk sac and migrate to the developing fetal liver, where they differentiate into erythroid, macrophage, and neutrophil lineages. Some blood cells also bud off as a result of EHT and form cell aggregates called hematopoietic clusters, which are later observed in several locations such as the dorsal aorta, vitelline artery, and umbilical artery. Hematopoietic clusters in these sites contain pre-HSCs which mature into fully functional HSCs before or after migration to the fetal liver (Yokomizo and Dzierzak 2010). Previously, it was thought that these functional, fetal liver HSCs then gradually replace EMPs and EMP-derived cells, before producing more defined hematopoietic progenitors, such as common myeloid progenitors, monocyte progenitors,

and multipotent progenitors. However, it is becoming increasingly clear that late gestational HSCs contribute less to the formation of downstream hematopoietic progenitors than previously believed. In vivo genetic tracing studies examining the early origins of hematopoietic progenitors in mice have demonstrated the simultaneous formation of HSCs and defined progenitors that were formerly considered descendants of HSCs (Yokomizo et al. 2022). One of the defined progenitors found to be generated without HSCs was multipotent progenitors, or MPPs.

Embryonic Multipotent Progenitors and Lymphoid Output

Previously, Patel et al. (2022) examined the developmental and clonal origins of adult blood progenitors in mice, using a cellular tagging system Sleeping Beauty which uniquely labels cells based on their individual transposon integration sites. Pregnant mice were first induced at five distinct time points: the stage of mesodermal specification which occurs at E6.5, the development of the hemogenic endothelium which occurs at E7.5, the early definitive wave which happens at E8.5, the mid-late definitive wave which happens at E9.5, and the fetal stage which occurs at E9.5. Researchers then sorted LT-HSCs, MPPs, and mature lineages, specifically granulocytes, B cells, monocytes, and megakaryocyte progenitors, from these mice and performed clonal analysis on the populations at three months. They observed that at earlier induction timepoints, most adult blood is derived from a pool of precursors that produce LT-HSCs, MPPs, and multilineage progeny, whereas in later time points, there was significant contribution from both LT-HSC and MPP clones. This was particularly significant as the MPP clones were unable to yield a corresponding tag for the HSC population and were therefore independent of HSCs, prompting investigators to define them as embryonic MPPs. In

addition, these embryonic MPPs, or eMPPs, were determined to produce a considerable fraction of mature cells at later induction timepoints, with a particular focus on the B-cell compartment. When the output of eMPP and LT-HSC clones was compared, 93.8% of mature cells were found to be generated by a LT-HSC clone but this contribution steadily decreased as the induction time point advanced, until reaching 8.25% in E13.5-induced mice. This was important because eMPP contribution, while initially minimal, gradually increased with later time points and was found to have produced 57% of mature lineages at the E13.5 induction time point (fig. 10A). Additionally, examination of the clonal contribution of HSCs and eMPPs in E13.5-induced three-month-old and one year-old mice revealed that though LT-HSC contribution to the B cell compartment was consistently low, eMPPs significantly contributed to the B cell pool at both three and twelve months of age (fig. 10B and 10C). These results were further confirmed when eMPPs were labeled with tdTomato and the presence of Tomato+ B cells, T cells, and granulocytes were observed over the course of a year. From this, Patel et al. (2022) found that eMPPs were primarily responsible for the production of B and T cells, which was indicated by their Tomato-positivity, but that the overall percentage of eMPP-derived lymphoid cells decreased with time (fig. 10D). These findings are consistent with other studies that have found HSC-independent MPP populations that continue into adulthood (Kobayashi et al. 2021; Dignum 2021). Collectively, this research suggests that eMPPs are a predominant source of lifelong lymphoid production, but that this output diminishes over time.

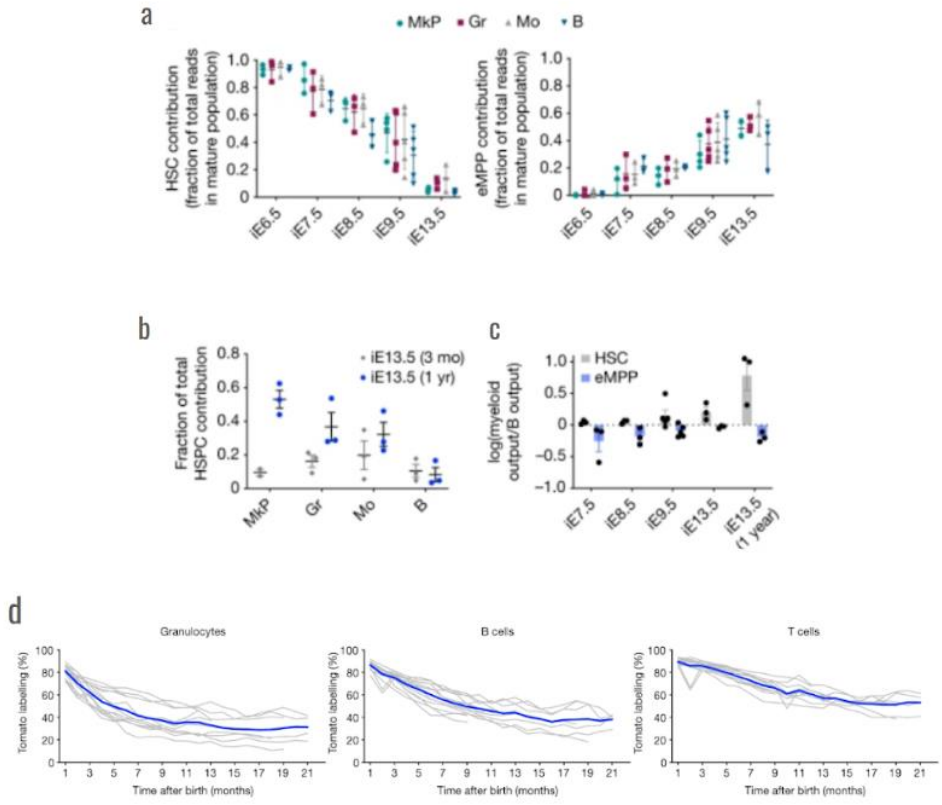

Figure 10. Embryonic Multipotent Progenitors and Contribution to Mature Lineages.

Fig. 10 demonstrates the output of eMPPs to mature lineages, compared to HSCs. Fig. 10A shows the fraction of reads in each mature cell populations that can be traced to either a LT-HSC or eMPP clone at three months of age. At earlier induction time points (iE6.5), there was significant HSC contribution, but this gradually decreased as the time points advanced. Embryonic MPPs, however, improved in later time points (iE13.5). Fig. 10B compares the HSC and eMPP contribution as a fraction of HSC and eMPP total output in megakaryocytes, granulocytes, monocytes, and B cells in three- and twelve-month-old mice that were induced at E13.5. Fig. 10C compares the myeloid and B cell output between HSCs and eMPPs at different induction points. HSC contribution towards myeloid cells increases as time points advance, but their contribution to the B cell compartment falls off. On the other hand, eMPPs produce more B cells than myeloid cells at both early and late time points. Notably, this production seems to decrease as the induction time points continue. Fig. 10D shows the percentage of eMPP-derived cells over time, indicated by their Tomato-positivity. Comparatively, the percentage of Tomato+ B and T cells seems to be higher than that of granulocytes but decreases over time. Retrieved from Patel, Sachin H., et al. "Lifelong multilineage contribution by embryonic-born blood progenitors." Nature, vol. 606, no. 7915, 2022, pp. 747-753, https://doi.org/10.1038/s41586-022-04804-z. Accessed 1 September 2023.

The introduction of embryonic multipotent progenitors poses serious implications for their role in the aged body's myeloid bias. As previously explained, the production of lymphoid and myeloid cells changes with age, with myeloid cells accounting for a higher percentage of peripheral blood in older individuals. This has mainly been researched with a focus on HSCs as they were thought to primarily produce lymphoid cells. However, the decreasing yet lifelong contribution of eMPPs to lymphoid output that Patel et al. (2022) observed challenges this idea. If eMPPs are a significant source of lymphoid cells but their contribution diminishes over time, this could be responsible for the reduced presence of lymphoid cells in aged peripheral blood and could result in the presentation of a myeloid skew. Therefore, this project examined the declining output of lymphoid cells by eMPPs and its potential role in myeloid bias, using an inducible CreER-LoxP recombination system that depleted the MPP population. Because MPPs have been found to be a predominant source of lymphoid cells, diminishing MPPs should in turn diminish lymphoid cells to the point that it imitates the myeloid skew. Overall, this project would illustrate the effects of MPP depletion on peripheral blood.

Chapter VII.

Methods

This project utilized an inducible CreER-loxP recombinase system to examine the observed skew from lymphoid to myeloid dominance.

MPPs and Myeloid Bias

Peripheral blood was collected from TAM-administered Flt3CreER|Tom/DTA mice and compared against samples from control Flt3CreER|Tom/Tom mice over a period of three months. Flt3CreER|Tom/DTA mice were designed for the targeted eradication of MPPs through the MPP-specific expression of Flt3 and the transcription of Diphtheria Toxin A, or DTA (Lai et al. 2005). Tamoxifen-dependent Cre activation results in the deletion of a lox-STOP-lox sequence and the transcription of tdTomato and DTA in the Rosa26 locus (fig. 11). DTA expression should result in the inhibition of protein synthesis, effectively killing the cell. However, if DTA was not properly transcribed, the cell would live. This aspect was particularly beneficial as it ensured the survival of a few MPPs, rather than completely decimating the entire population, and therefore directly mimicked the aged body's lymphoid depletion. Additionally, the surviving MPP, and any of its subsequent progeny, would be able to be fluorescently imaged due to tdTomato. Tomato therefore served as a positive control to demonstrate the contribution of the few MPPs that were affected and survived. Furthermore, this design allowed the use of young mice, despite the myeloid skew typically only being seen in aged mice. This was important because there would not be any secondary effects of old age, such as inflamed bone marrow, in the young mice which would have been

present if old mice had been used. Therefore, any results would be directly produced by the MPP depletion. Lastly, this system was advantageous as it is both tissue-specific as Flt3 is a protein that is only found in MPPs and time-sensitive as it is dependent on Tamoxifen administration. Additionally, using Flt3CreER|Tom/Tom mice as controls demonstrated that the DTA expression was causing the MPP depletion, and not the CreER recombinase system itself.

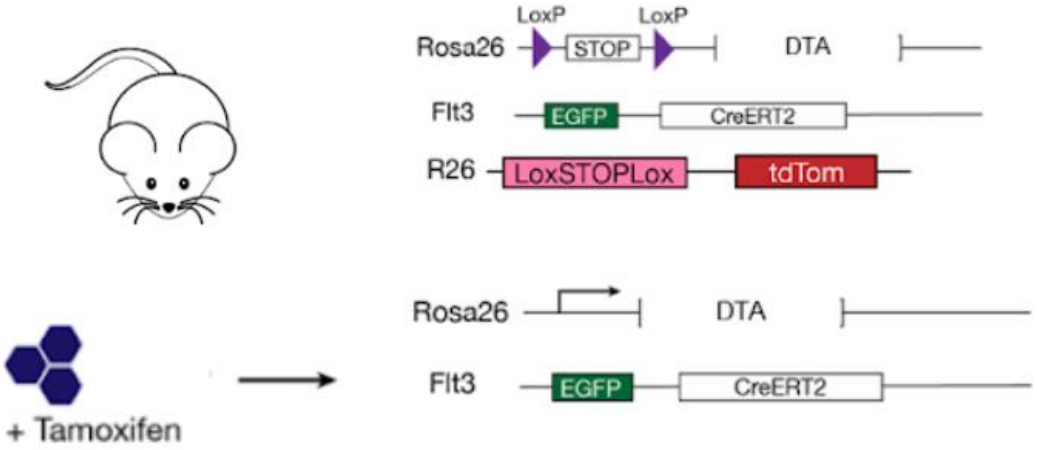

Figure 11. Flt3CreER-Lox System.

Fig. 11 illustrates how the Flt3CreER-Lox system works. In the Rosa 26 loci, there is a lox-STOP-lox sequence. Under normal conditions, everything downstream of the lox-STOP-lox locus will be ignored during transcription. However, when treated with Tamoxifen, CreER will excise the STOP locus, allowing the transcription of tdTomato and DTA. This will result in widespread eMPP death but those that survive, and their subsequent progeny will be fluorescently labeled as red. Created using BioRender.com, accessed 28 November 2023.

After TAM injection, retro-orbital blood collections were performed on the Flt3CreER|Tom/DTA and control mice at one month, two months, and three months

post-injection. Peripheral blood samples were purified with RBC lysis and stained with fluorescent antibodies for myeloid and lymphoid cells. Myeloid cell markers included CD45, which was used to recognize all nucleated hematopoietic cells as it is a common antigen, and Ter119, which was used to exclude erythrocytes and target the relevant cell populations. CD61 and Ly6G were also used for the detection of platelets and granulocytes. Lymphoid cell markers included Ter119 also for the exclusion of erythrocytes, CD8a and CD4 for the identification of T cells, and CD19 to distinguish B cells. Flow cytometry was then performed on the samples and the relevant cell populations were identified and recorded. With this, the blood progenitors in Flt3CreER|Tom/DTA mice were compared to those in control mice, which were treated as a biological standard as they had not experienced depletion. Overall, these experiments allowed me to determine whether the depletion of multipotent progenitors plays a role in myeloid population predominance.

Mouse Model

Flt3CreER|Tom/DTA and Flt3CreER|Tom/Tom mice were used. Mice were crossed and genotyped using PCR-based assays with tail DNA samples, prior to starting the experiment. Cre activation was induced by a single intraperitoneal injection of 40 mg of TAM.

Flow Cytometry

At 1 month, 2 months, and 3 months post-TAM administration, peripheral blood was collected through the retro-orbital sinus. At least two capillaries of blood were obtained and preserved using an anticoagulation buffer. Red blood cells were removed

using density-separation and RBC lysis buffer for 15 minutes. At which point, non-RBC fractions were collected, centrifuged, and resuspended in PBS. Samples were then stained with several fluorescent antibodies for 40 minutes. As previously described, the myeloid antibody cocktail consisted of Ter119, CD45, CD61, and Ly6G, whereas the lymphoid cell markers included Ter119, CD8a, CD4, and CD19. PE and GFP positivity were also recorded and accounted for. Single-color and no-color controls were used to ensure correct voltage and compensation setup. Flow cytometry was performed on a FACSAria instrument and data was analyzed with FlowJo software.

Chapter VIII.

Results

The previously described procedures for peripheral blood collection and preparation were performed and produced the following results.

MPPs and Myeloid Bias

In order to establish the influence of MPP depletion on peripheral blood and its possible role in myeloid population predominance, this project examined lymphoid and myeloid cells in Flt3CreER|Tom/DTA and Flt3CreER|Tom/Tom mice over a three-month period.

Lymphoid Cell Flow Cytometry

The peripheral blood of induced Flt3CreER|Tom/DTA and control mice was examined using cell surface markers corresponding to lymphoid cell populations at 1 month, 2 months, and 3 months post-Tamoxifen administration. Specifically, Tomato+ T cells were analyzed based on the expression of CD4 and/or CD8, as well as Tomato+ B cells using the cell surface marker CD19. Figure 12 shows the flow cytometry gating strategy used to analyze these populations, which consisted of forward scatter and side scatter density graphs to determine the overall cell population of interest. Following these graphs, the positive selection for Tomato-expressing cells and the negative selection of Ter119-expressing cells was done. From this gating, the T cell population was derived (fig. 12). As mentioned previously, the T cell subtype was established from the expression of CD4 and/or CD8a. However, cells that were negative for both the CD4 and

CD8 markers, or the ‘double-negative’ population, were then analyzed for CD19 expression to identify B cells. All FACS data examining lymphoid cells in mice over the 3-month period used this gating design (fig. 12).

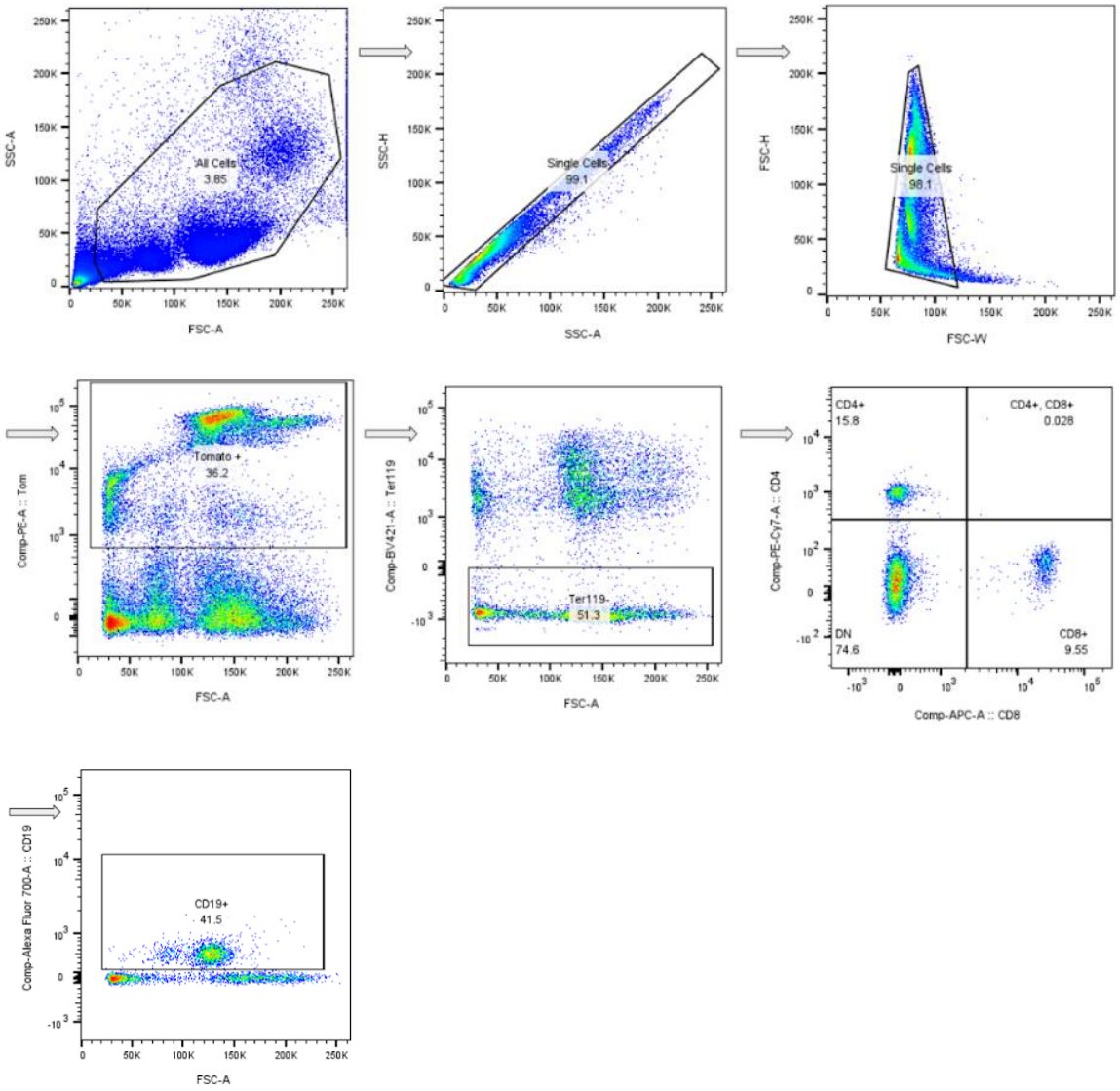

Figure 12. Lymphoid Cell Flow Cytometry Gating.

Fig. 12 demonstrates the gating strategy used to identify the lymphoid cell populations. Cells were first gated based on their forward (FSC-A) and side scattering (SSC-A).

Doublets were then excluded, using side scatter height (SSC-H) versus side scatter area (SSC-A) and forward scatter height (HSC-H) versus forward scatter width (FSC-W). Next, all Tomato+ cells were identified, from which erythroid cells were excluded (Ter119-). From this, the T cell population was established, with the expression of CD4+ and/or CD8+ indicating the T cell subtype that the cell is associated with. Double-negative (DN) cells, meaning they expressed neither CD4 nor CD8, provided the basis for the discovery of the B cell population, which was determined by the positive selection of CD19-expressing cells (CD19+).

Peripheral blood was first collected one month after Tamoxifen had been administered to experimental and control mice. Figure 13 depicts the flow cytometric analysis of peripheral blood samples from 2 Flt3CreER|Tom/DTA and 2 Flt3CreER|Tom/Tom mice at this time point. Flt3CreER|Tom/Tom mice all exhibited higher levels of Tomato+ cells compared to Flt3CreER|Tom/DTA samples. Additionally, of these Tomato+ cells, it was determined that the majority were erythrocytes in FLt3CreER|Tom/Tom mice. Regarding Tomato+ T cells, there were unfortunately varied levels of CD4+ T cells among Flt3CreER|Tom/DTA samples, but control samples displayed consistently low levels in the population. Flt3CreER|Tom/DTA samples also had inconsistent numbers in the ‘double-negative’ quadrant yet displayed similar numbers for the CD8+ only and both CD4+ and CD8+ populations. Because of this, it is possible that in the second Flt3CreER|Tom/DTA mouse shown (fig. 13), the cell marker staining for CD4 did not properly mark some of the CD4-expressing cells, leading them to be improperly labeled as double-negative. This would mean that the number of CD4+ cells in the first Flt3CreER|Tom/DTA mouse (fig. 13) is accurate and that there are considerably more CD4+ cells in Flt3CreER|Tom/DTA samples than in control samples at 1 month. Despite the discrepancy of CD4+ and double-negative cells among experimental mice, there was a similar proportion of CD19+ B cells observed in both

Flt3CreER|Tom/DTA mice. Flt3CreER|Tom/Tom samples, on the other hand, had much lower CD19+ cell percentages (fig. 13).

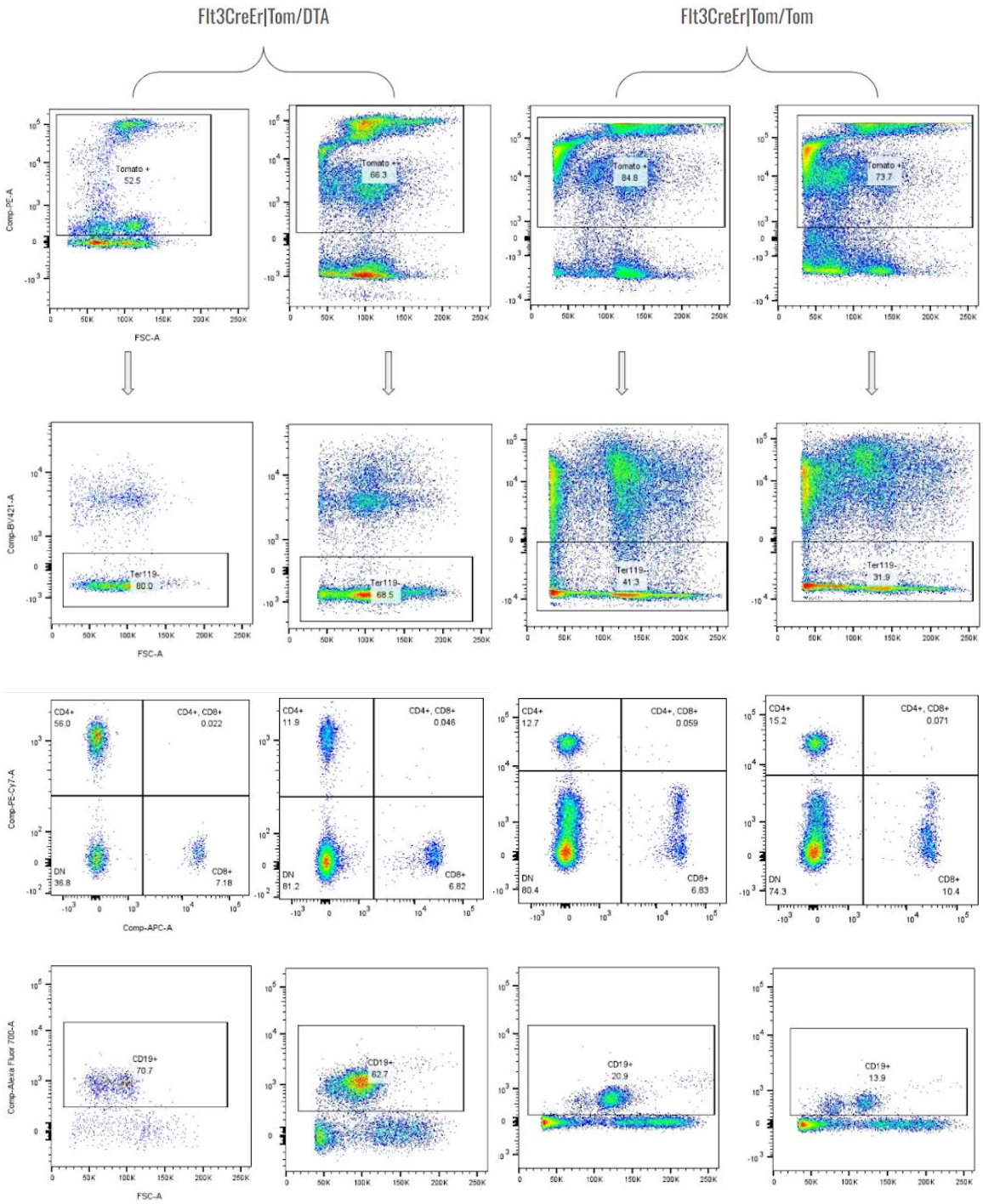

Figure 13. Representative Image of 1 Month Lymphoid Cells.

Fig. 13 shows the flow cytometric analysis cells in peripheral blood from Tamoxifen-administered Flt3CreER|Tom/DTA and Flt3CreER|Tom/Tom mice, 1-month post-

injection. After forward and side scatter gating and the exclusion of doublets (not shown), Tomato+ cells were then identified. As illustrated in the figure, there was a higher proportion of Tomato+ cells in the Flt3CreER|Tom/Tom samples than the Flt3CreER|Tom/DTA. Conversely, the Flt3CreER|Tom/DTA had more Ter119- cells than the Flt3CreER|Tom/Tom ones. Regarding CD4+ cells, Flt3CreER|Tom/DTA mice had consistent, low numbers whereas Flt3CreER|Tom/DTA mice had a bit of a discrepancy. CD8+ cells were fairly similar between experimental and control samples. CD19+ B cells showed a much higher count in Flt3CreER|Tom/DTA mice than in Flt3CreER|Tom/Tom ones.

Flt3CreER|Tom/DTA and Flt3CreER|Tom/Tom mice were then examined at 2 months post-Tamoxifen injection. Comparing the one and two-month timepoints, Flt3CreER|Tom/Tom samples retained the Tomato+ dominance that had been observed at 1 month. However, the proportion of Tomato+ cells among Flt3CreER|Tom/Tom samples were considerably lower (fig. 14). On the other hand, the Ter119- dominance that had been seen among Flt3CreER|Tom/DTA mice was significantly higher at the 2-month timepoint. For the T cell population, the CD4+, CD8+, and double-positive populations were similar among both Flt3CreER|Tom/DTA and Flt3CreER|Tom/Tom samples. The double-negative population was also consistent among experimental and control samples. Although, the CD19+ B cell count, which is gated from the double-negative population, was significantly higher in Flt3CreER|Tom/DTA mice (fig. 14).

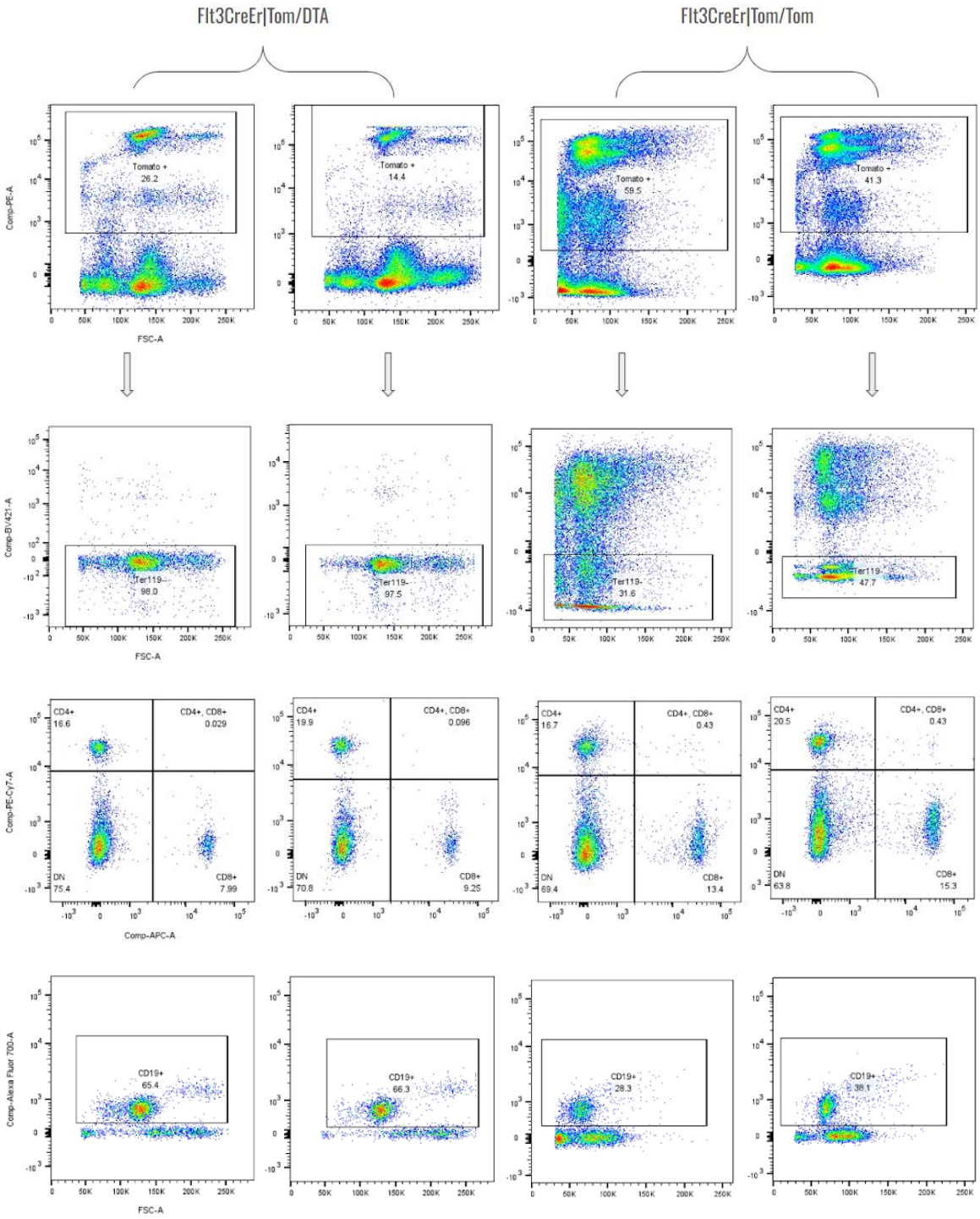

Figure 14. Representative Image of 2 Month Lymphoid Cells.

Fig. 14 illustrates the flow cytometric analysis of lymphoid cells in peripheral blood from Flt3CreER|Tom/DTA and Flt3CreER|Tom/Tom mice that had been injected with

Tamoxifen 2 months prior. After forward and side scatter gating and the exclusion of doublets (not shown), Tomato+ cells were then identified. It was found that while Flt3CreER|Tom/Tom samples had more Tomato+ cells than Flt3CreER|Tom/DTA samples, Flt3CreER|Tom/DTA samples had more Ter119- cells. Furthermore, the proportion of CD4+ and/or CD8+ T cells was consistent among both Flt3CreER|Tom/DTA and Flt3CreER|Tom/Tom samples. The samples also had a consistent number of cells that were 'double-negative' (DN). However, among this double-negative population, there was a considerable difference between the number of B cells, marked by CD19, in Flt3CreER|Tom/DTA versus Flt3CreER|Tom/Tom mice.

At 3 months post-Tamoxifen administration, Flt3CreER|Tom/DTA and Flt3CreER|Tom/Tom mice were analyzed a final time. Compared to Flt3CreER|Tom/DTA samples, Flt3CreER|Tom/Tom samples were still found to have a higher number of Tomato+ cells, with levels similar to those seen at 2 months (fig. 15). Interestingly, at the three-month timepoint, the Ter119- dominance of Tomato+ cells that had been exhibited in Flt3CreER|Tom/DTA mice at one and two months was now seen in control mice. In regard to the T cell population, there were similar levels of CD4+ and/or CD8+ cells in 2 and 3 months in both Flt3CreER|Tom/DTA and Flt3CreER|Tom/Tom mice. In the CD19+ population, there was a slight difference in Flt3CreER|Tom/DTA samples that was not seen in experimental samples. Furthermore, in Flt3CreER|Tom/Tom mice, there was an increase in the CD19 B cell type between the second and third months.

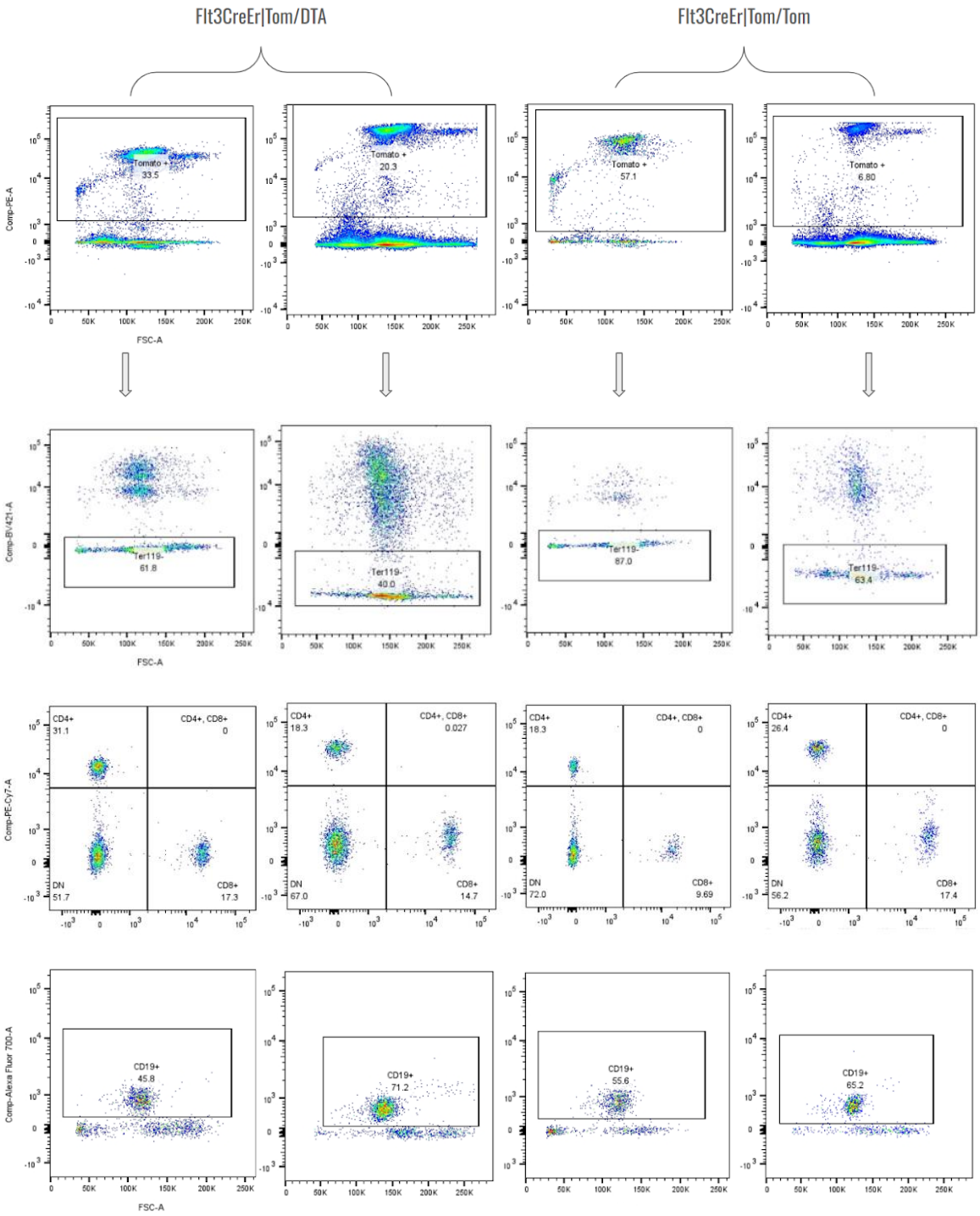

Figure 15. Representative Image of 3 Month Lymphoid Cells.

Fig. 15 depicts the flow cytometric analysis of lymphoid cells in peripheral blood from Tamoxifen-administered Flt3CreER|Tom/DTA and Flt3CreER|Tom/Tom mice 3 months

post-injection. After forward and side scatter gating and the exclusion of doublets (not shown), Tomato+ cells were then identified and Flt3CreER|Tom/Tom samples were observed as having a higher Tomato+ population. Flt3CreER|Tom/Tom samples also had a higher Ter119- population as well. The CD4+ and/or CD8+ T cell populations had low proportions across Flt3CreER|Tom/DTA and Flt3CreER|Tom/Tom samples, with one Flt3CreER|Tom/DTA sample having a slightly higher CD4+ count and with Flt3CreER|Tom/DTA samples overall having higher CD8+ counts. Among the CD19+ population, there was a slight difference among experimental samples, but controls exhibited fairly similar levels.

After acquiring all flow cytometry data over the three-month period, it was examined for potential changes to the lymphoid cell populations. Taking the percentages of each cell type observed in all Flt3CreER|Tom/DTA and Flt3CreER|Tom/Tom mice included in the study, figure 16 shows an average of the cell type percentages at the 1 month, 2 month, and 3-month timepoints. In regard to the Tomato+ population, Flt3CreER|Tom/Tom mice displayed comparatively higher levels of Tomato+ cells that steadily decreased over the three months (fig. 16A). Of the Tomato+ cells, erythroid cells accounted for a greater percentage of the compartment in Flt3CreER|Tom/Tom samples, whereas Flt3CreER|Tom/DTA samples had an overwhelming majority of Ter119- cells (fig. 16B). Notably, Flt3CreER|Tom/DTA mice displayed the highest percentage of Ter119- cells at the 2-month timepoint, with an average of 97.75% of the Tomato+ population. From the Tomato+, Ter119- compartment, the CD4+ T cell subtype suggested a kind of inverse relationship between the Flt3CreER|Tom/DTA and Flt3CreER|Tom/Tom mice. At 1 month, CD4+ T cells represented an average of 34% in Flt3CreER|Tom/DTA samples, but only 14% in Flt3CreER|Tom/Tom samples (fig. 16C). By 2 months, however, the proportion of CD4+ cells in experimental mice decreased while the levels in control mice increased. Similarly, at 3 months, when the CD4+ T cell count increased in Flt3CreER|Tom/DTA mice, it decreased in Flt3CreER|Tom/Tom

mice. CD8+ T cells, on the other hand, gradually increased in Flt3CreER|Tom/DTA samples (fig. 16D). In Flt3CreER|Tom/Tom samples, there was an increase between the first two months, with a slight decrease at the third month. In regard to the proportion of CD19+ B cells within the double-negative compartment, there were fairly steady numbers throughout the 3 months period among samples from Flt3CreER|Tom/DTA mice (fig. 16E). Conversely, Flt3CreER|Tom/Tom mouse samples displayed a prolonged increase in the percentage of CD19+ cells.

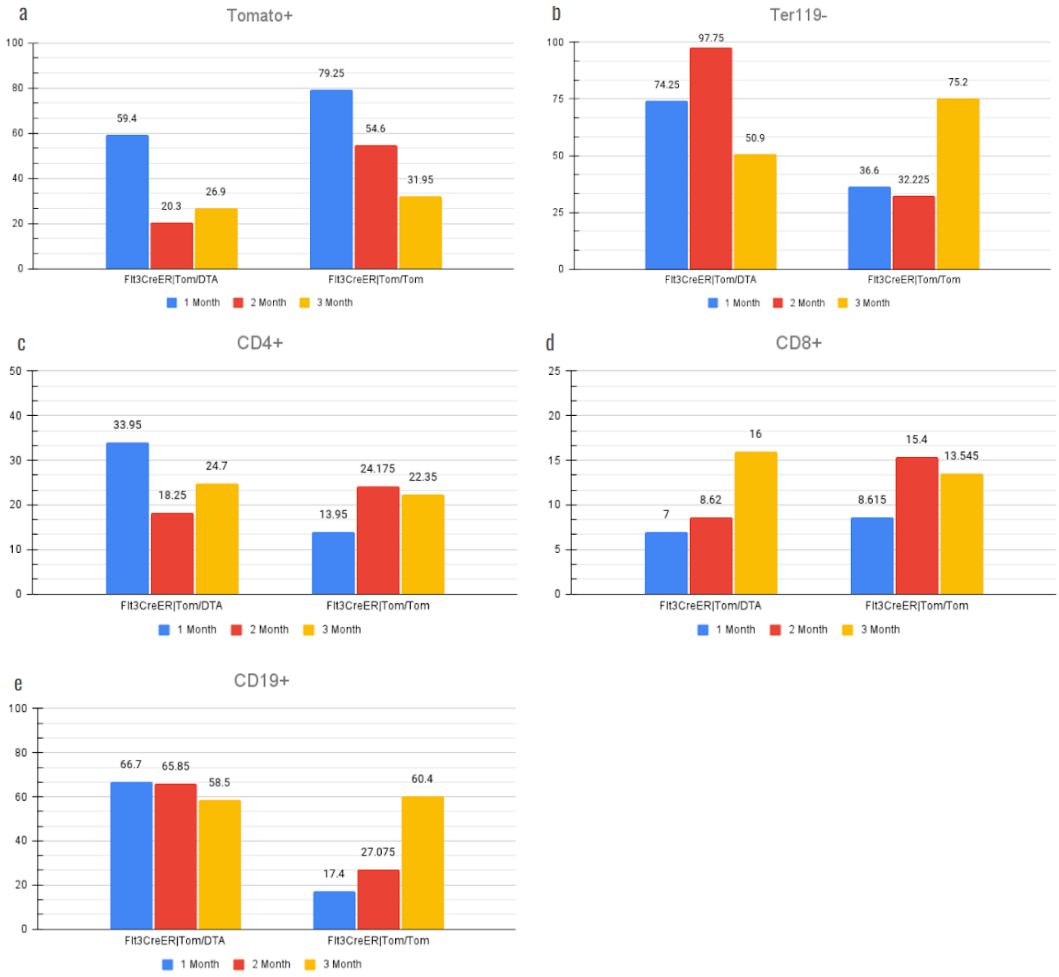

Figure 16. Overall Changes to Lymphoid Cell Populations.

Fig. 16 presents the average percentages of each lymphoid cell type based on all of the Flt3CreER|Tom/DTA and Flt3CreER|Tom/Tom mice examined at the 1 month, 2 month, and 3-month timepoints. Fig. 16A shows the average number of Tomato+ cells in Flt3CreER|Tom/DTA mice versus Flt3CreER|Tom/Tom mice across the three-month time span. For Flt3CreER|Tom/DTA samples, Tomato+ cells made up an average of 59.4% (SD = 9.758) of all cells at 1 month, then later dropping to 20.3 ± 8.344 at 2 months. Flt3CreER|Tom/Tom samples also exhibited a slight decline in the Tomato+ cell population between 1 and 2 months, going from 79.25% (SD = 7.849) to 54.6% (SD = 11.573). However, at three months, Tomato+ cells accounted for similar levels in experimental (26.9 ± 9.334) and control samples (31.95 ± 35.567). Fig. 16B illustrates the change of the Tomato+ Ter119- compartment over time. Flt3CreER|Tom/DTA mice had 74.25% (SD = 8.132) at 1 month and increased to 97.75% (SD = 0.354) at 2 months. The Ter119- compartment then dropped to 50.9% (SD = 15.415) of the Tomato+ population. Conversely, Flt3CreER|Tom/Tom samples had lower levels of Ter119- cells

(36.6 ± 6.647) at 1 month and slightly decreased (32.225 ± 11.385) at 2 months. However, at 3 months, the presence of Ter119- cells significantly increased to 75.2% (SD = 16.688), directly opposing the changes seen in Flt3CreER|Tom/Tom mice. Fig. 16C depicts the average percentage of CD4+ T cells detected in experimental and control mice. The number of CD4+ T cells in Flt3CreER|Tom/DTA samples shifted from 33.95% (SD = 31.183) to 18.25% (SD = 2.333), before ending up at 24.7% (SD = 9.051), over the 3-month period. Flt3CreER|Tom/Tom samples, on the other hand, exhibited low CD4+ counts (13.95 ± 1.768) at 1 month that slightly increased (24.175 ± 8.512) at 2 months. Though, it ultimately lowered to 22.35% (SD = 5.728). On the other hand, CD8+ T cells steadily increased in Flt3CreER|Tom/DTA mice (fig. 16D). At 1 month, CD8+ T cells represented merely 7% of the population (SD = 0.255) and only increased to 8.62% (SD = 0.891) at 2 months. However, by 3 months, CD8+ T cell numbers doubled (16 ± 1.838). In Flt3CreER|Tom/Tom samples, CD8+ T cells increased between 1 month (8.615 ± 2.524) and 2 months (15.4 ± 3.236). At 3 months, the percentage of CD8 T cells slightly decreased to 13.545% (SD = 5.452). Fig. 16E shows the changes in the presence of CD19+ B cells. In experimental samples, the percentage of CD19 B cells was fairly consistent throughout the 3 months. On average, CD19 B cells represented 66.7% (SD = 5.657) of the population at 1 month, 65.85% (SD = 0.637) at 2 months, and 58.5% (SD = 17.961) at 3 months. In control samples, a steady increase in the CD19 B cell count was observed, starting at 17.4% (SD = 4.950), then increasing to 27.075% (SD = 8.773), and ending up at 60.4% (SD = 6.788).

Myeloid Cell Flow Cytometry

The peripheral blood of Tamoxifen-administered experimental and control mice was also examined for myeloid cell populations over the 3-month time period. Tomato+ granulocytes were recognized using the surface marker Ly6G, and Tomato+ megakaryocytes and platelets were identified using CD61. Figure 17 illustrates the FACS gating strategy used to analyze these cell types. In addition to the standard forward scatter and side scatter density graphs, the expression of the CD45 surface marker was used to further exclude cellular debris and restrict hematopoietic cells from the total events recorded. All FACS data examining lymphoid cells in mice over the 3-month period used this gating design.

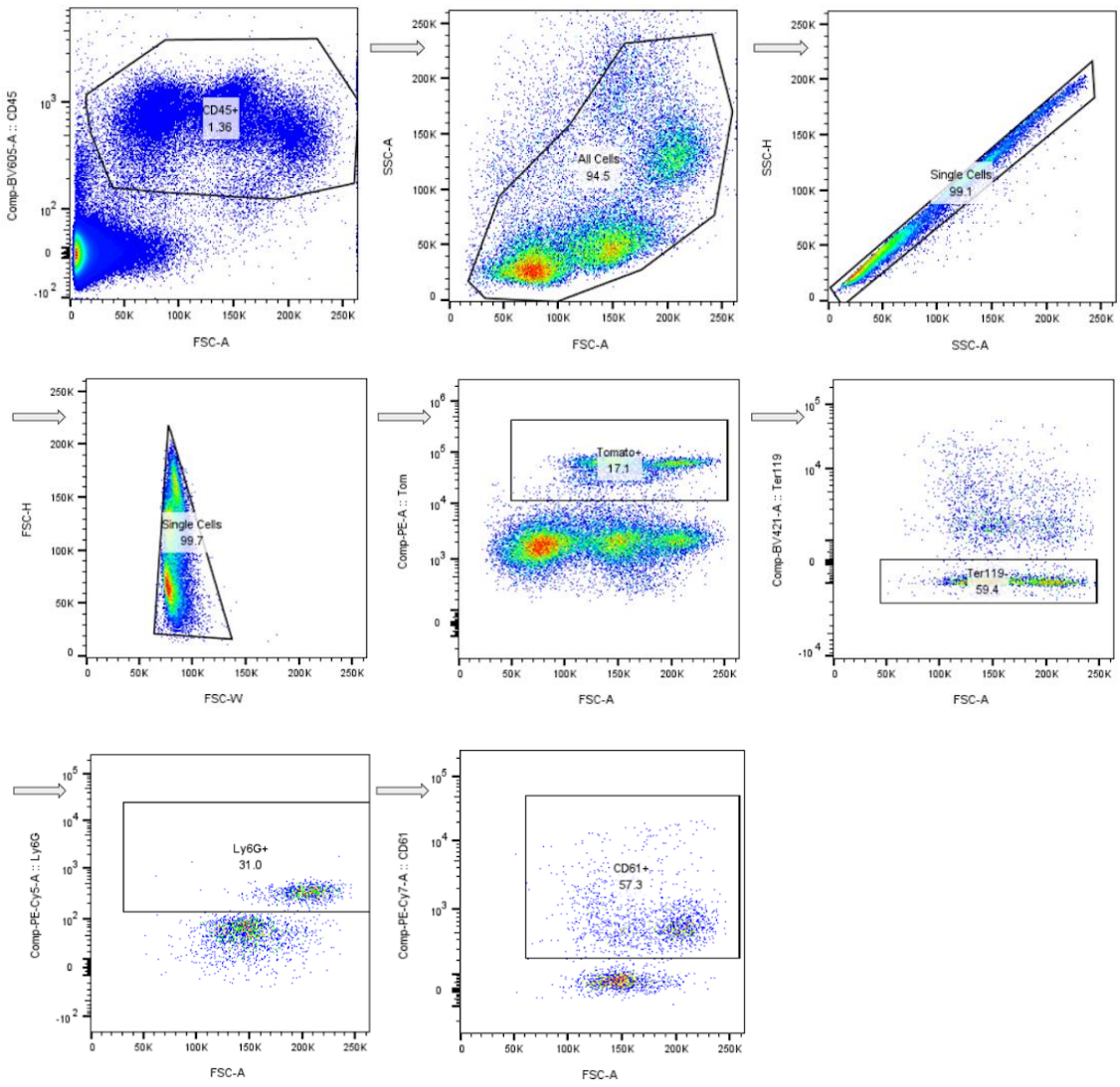

Figure 17. Myeloid Cell Flow Cytometry Gating.

Fig. 17 represents the gating strategy used to identify the myeloid cell populations. Initially, cells were gated based on CD45 expression (CD45+) and on their forward (FSC-A) and side scattering (SSC-A). Doublets were then excluded, using side scatter height (SSC-H) versus side scatter area (SSC-A) and forward scatter height (FSC-H) versus forward scatter width (FSC-W). Next, the positive selection of Tomato cells (Tomato+) and the negative selection of erythroid cells (Ter119-) were used to further narrow the relevant populations. Granulocytes were recognized based on the expression of Ly6G (Ly6G+). Additionally, platelets and megakaryocytes were identified based on CD61 expression (CD61+).

Tomato+ myeloid cells in Flt3CreER|Tom/DTA and Flt3CreER|Tom/Tom mice were first analyzed at the 1-month timepoint, the results of which are shown in figure 18. As previously explained, the Tomato+ cells were obtained from the general CD45+, single cell population. Within experimental and control groups, corresponding percentages were observed, with the Flt3CreER|Tom/Tom samples displaying significantly higher levels of Tomato+ cells compared to Flt3CreER|Tom/DTA ones. From the Tomato+ cell group, the Ter119- population was determined which also had comparable levels between both experimental and control mice. In regard to the Tomato+ Ly6G+ granulocytes, Flt3CreER|Tom/Tom samples demonstrated similar, and generally higher, numbers. The Flt3CreER|Tom/DTA samples, on the other hand, had relatively inconsistent results. Furthermore, the CD61 surface marker expression graphs for Flt3CreER|Tom/DTA and Flt3CreER|Tom/Tom samples did not depict distinct positive populations. Unfortunately, this was a characteristic observed in the second and third month timepoints as well and likely due to mistakenly identifying a different CD61-expressing cell type as macrophages or platelets. Because of this, these results were not included in the later timepoints.

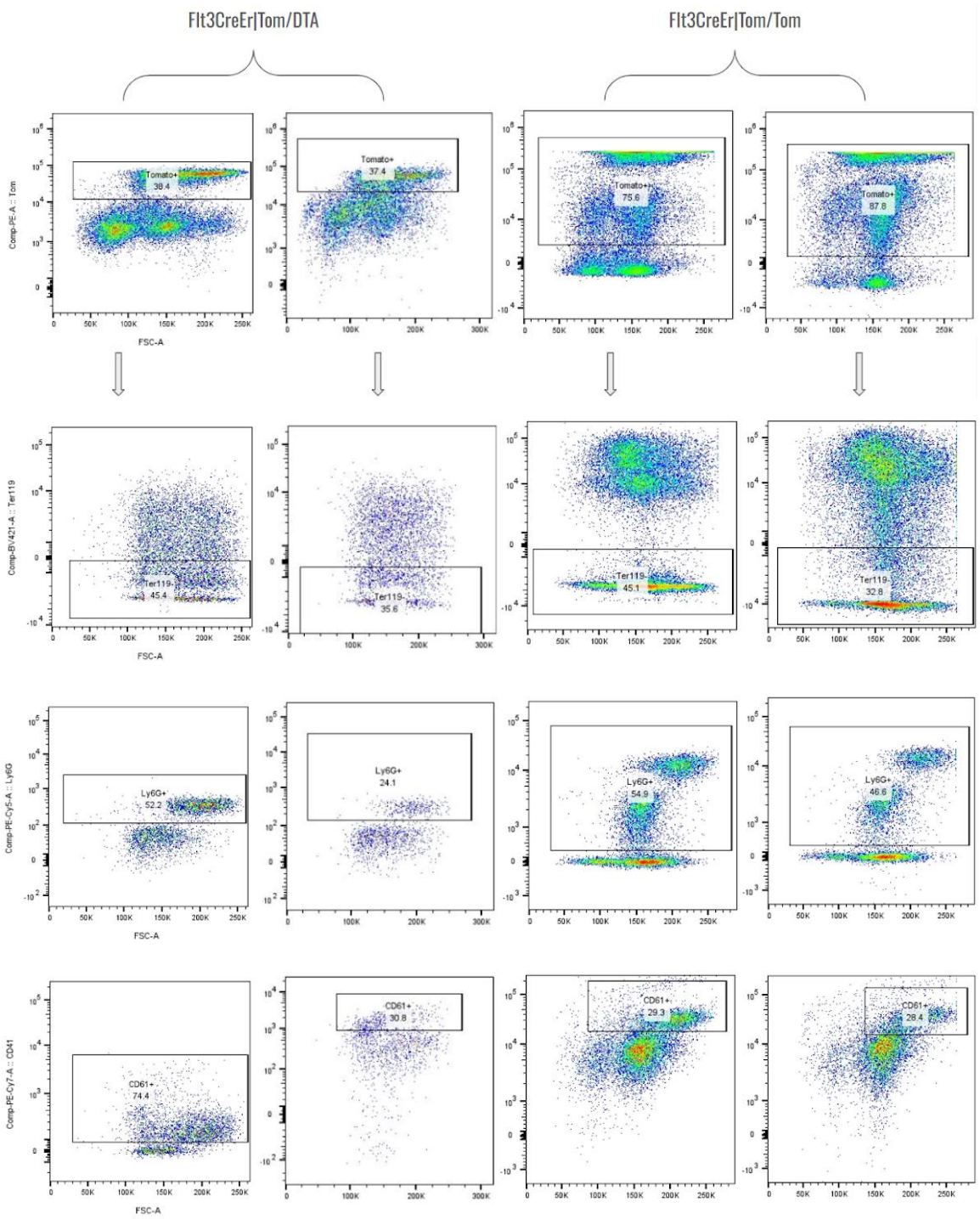

Figure 18. Representative Image of 1 Month Myeloid Cells.

Fig. 18 illustrates the flow cytometric analysis of myeloid cells in peripheral blood from Tamoxifen-administered Flt3CreER|Tom/DTA and Flt3CreER|Tom/Tom mice at 1-month

post-injection. Following the CD45 expression graph and the forward scatter and side scatter density graphs (not shown), the Tomato+ cell population was identified. Both Flt3CreER|Tom/DTA samples had similar Tomato+ counts, and the Flt3CreER|Tom/Tom samples also displayed similar counts to one another. This was also the case for the Ter119- cell population. For the Ly6G+ granulocytes, Flt3CreER|Tom/Tom mice exhibited similar percentages, whereas Flt3CreER|Tom/DTA mice had a slight difference in numbers. Regarding the marker CD61, there was not a well-defined positive population among any samples.

By the second month, Tomato+ cells represented a smaller portion of Flt3CreER|Tom/Tom mice (fig. 19), compared to the first month flow cytometry data. Despite this, Flt3CreER|Tom/Tom samples still maintained the previously observed Tomato+ cell predominance. In addition to this, the Ter119- population was greater in experimental mice than in controls. In regard to granulocytes, Ly6G+ cells substantially decreased between the first and second months in both Flt3CreER|Tom/DTA and Flt3CreER|Tom/Tom samples (fig. 19). Additionally, while Flt3CreER|Tom/Tom samples had more Ly6G+ cells at 1 month, Flt3CreER|Tom/DTA samples had more at 2 months.

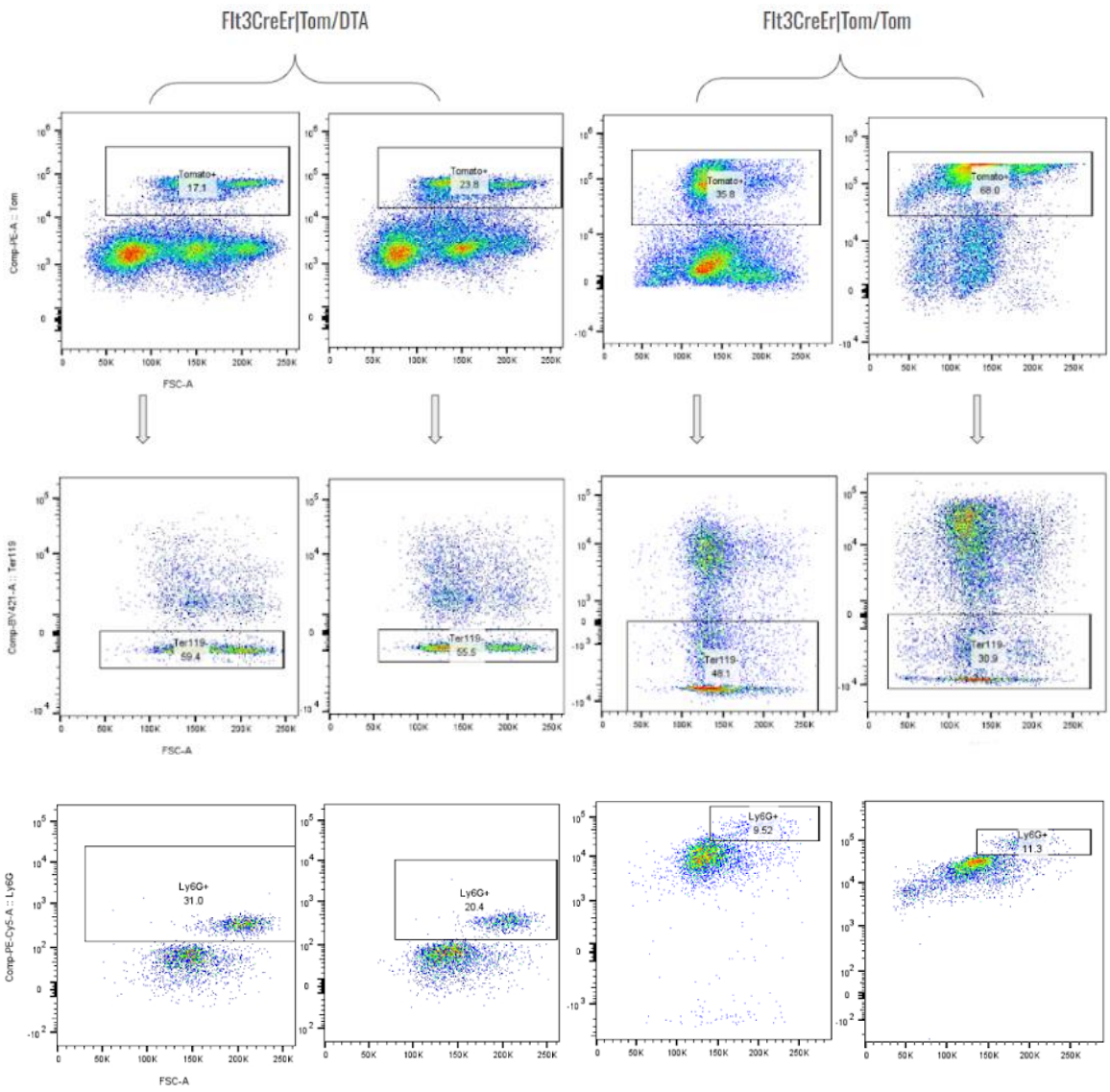

Figure 19. Representative Image of 2 Month Myeloid Cells.

Fig. 19 demonstrates the examination of myeloid cells in peripheral blood samples from Flt3CreER|Tom/DTA and Flt3CreER|Tom/Tom mice, 2 months after Tamoxifen injections. Following density plots (not shown), Tomato+ cells were identified and determined to be more prevalent in Flt3CreER|Tom/Tom samples compared to Flt3CreER|Tom/DTA samples. However, there was a light difference in Tomato+ numbers between Flt3CreER|Tom/Tom samples. Additionally, Flt3CreER|Tom/DTA were seen to have more Ter119- cells. In regard to the granulocyte population, Ly6G-expressing cells made up a higher proportion of Tomato+, Ter119- cells in Flt3CreER|Tom/DTA mice versus Flt3CreER|Tom/Tom mice.

The presence of myeloid cells in Flt3CreER|Tom/DTA and Flt3CreER|Tom/Tom mice was examined a final time at 3 months post-Tamoxifen administration. Both experimental and control mice exhibited lower levels of Tomato positivity, with Flt3CreER|Tom/Tom mice still maintaining more Tomato+ cells than Flt3CreER|Tom/DTA mice. Of the Tomato+ cells, Flt3CreER|Tom/Tom samples exhibited a slight decrease in Ter119- cells, compared to the second month timepoint. Moreover, Flt3CreER|Tom/DTA samples shows a slight discrepancy in the percentages of the Ter119- cell population. Notably, Ly6G+ granulocytes had significantly diminished in all samples.

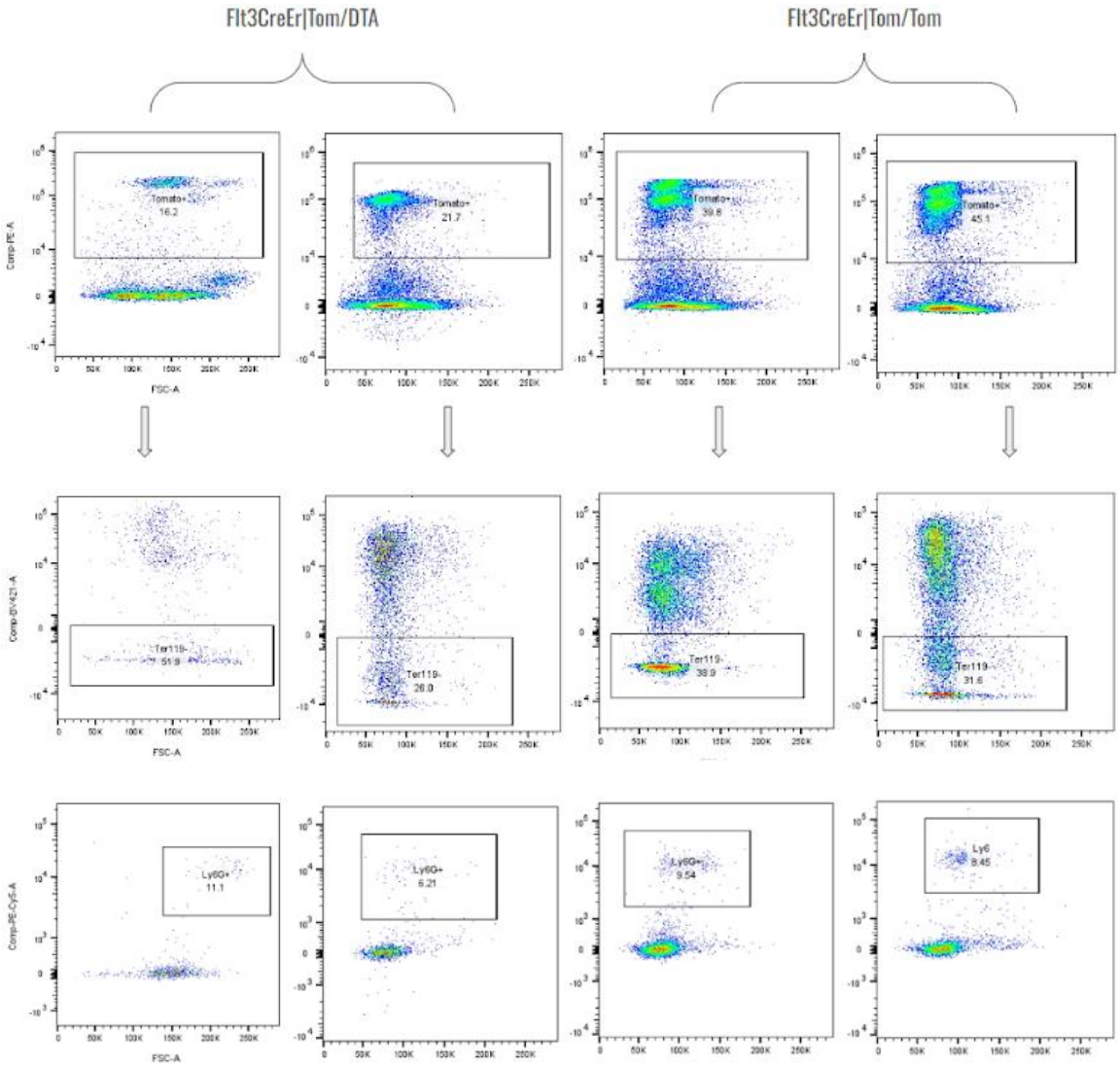

Figure 20. Representative Image of 3 Month Myeloid Cells.

Fig. 20 depicts the examination of myeloid cells from Flt3CreER|Tom/DTA and Flt3CreER|Tom/Tom mice that had been injected with Tamoxifen 2 months prior. After the positive selection for CD45-expressing cells and the exclusion of doublets (not shown), Tomato+ cells were examined and found to be more prominent in Flt3CreER|Tom/Tom samples. The proportion of Ter119- cells among Flt3CreER|Tom/DTA mice were slightly varied, whereas Flt3CreER|Tom/Tom samples showed similar levels. Lyg6+ cells were largely absent in all samples, regardless of experimental or control status.

Following the collection of all flow cytometry data over the three-month period, it was analyzed for possible changes to the myeloid cell types. Calculating the individual percentages for the Tomato+, Ter119-, and Ly6G+ cell populations reported amongst all experimental and control mice involved in the study, figure 21 shows an average of these percentages at the various timepoints. Comparing the Flt3CreER|Tom/DTA and Flt3CreER|Tom/Tom Tomato+ fraction, a prevalent Tomato+ population that steadily decreased over the three months was seen in Flt3CreER|Tom/Tom samples (fig. 21A). Flt3CreER|Tom/DTA samples, on the other hand, had notably lower numbers of Tomato+ cells. The Tomato+ Ter119- population between experimental and control groups was very similar at 1 month (fig. 21B). However, at 2 months, the Ter119- population increased in Flt3CreER|Tom/DTA mice yet remained the same in Flt3CreER|Tom/Tom mice. By month 3, this difference in percentages resolved as the Ter119- count in Flt3CreER|Tom/DTA samples dropped to that of Flt3CreER|Tom/Tom samples. Of this Tomato+ Ly6G+ granulocyte population, Flt3CreER|Tom/Tom mice initially displayed considerably high percentages of Ly6G+ cells at 1 month, which significantly dropped at the second and third months (fig. 21C). Flt3CreER|Tom/DTA also experienced a decline in Ly6G+ cells over the three-month period, but it was distinctively more gradual in comparison.

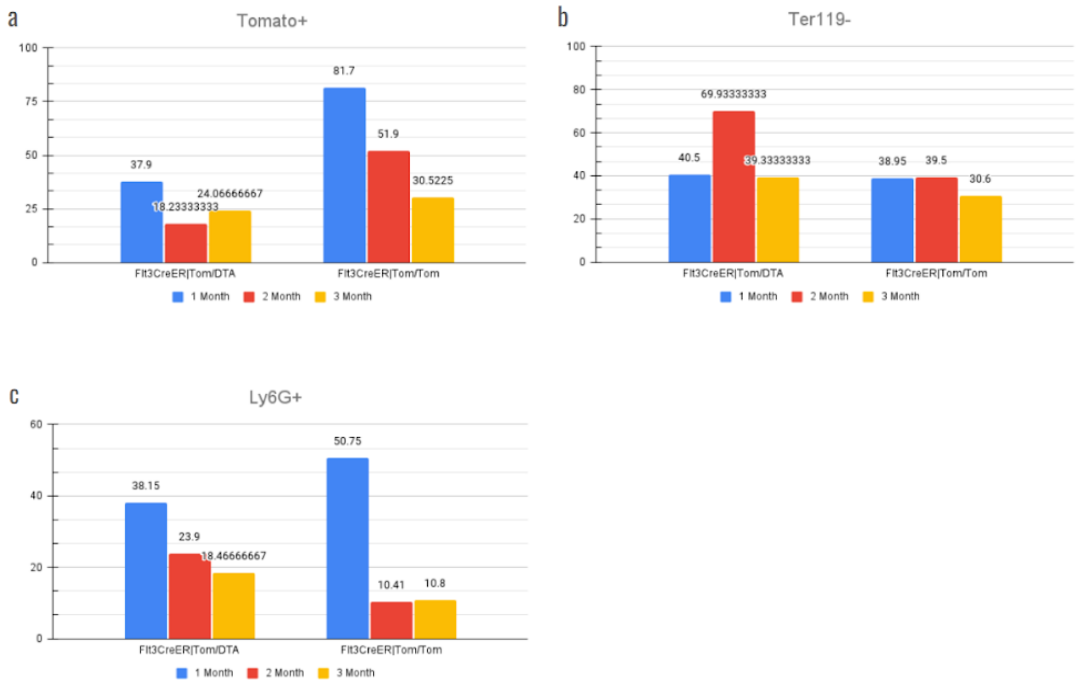

Figure 21. Overall Changes to Myeloid Cell Populations.

Fig. 21 presents the average percentages of each cell population based on all of the Flt3CreER|Tom/DTA and Flt3CreER|Tom/Tom mice examined at the 1 month, 2 month, and 3-month timepoints. Fig. 21A displays the average number of Tomato+ cells found within the CD45+, single cell population among all experimental and control mice examined at each timepoint. In Flt3CreER|Tom/DTA mice, there were low levels of Tomato+ cells at all timepoints, starting at 37.9% (SD = 0.707) and then falling to 18.233% (SD = 5.095) before ending up at 24.067% (SD = 10.543). Flt3CreER|Tom/Tom samples, though, initially had high Tomato+ levels (81.7 ± 8.627) which gradually decreased (51.9 ± 22.769) until reaching half of the original amount (30.523 ± 17.090). Fig. 21B depicts the average percentage of Ter119- cells found within the Tomato+ population in all Flt3CreER|Tom/DTA and Flt3CreER|Tom/Tom mice included in the experiment. In samples from Flt3CreER|Tom/DTA mice, Ter119- cells were responsible for 40.5% (SD = 6.930) of the Tomato+ population at 1 month, 69.933% (SD = 21.710) at 2 months, and 39.333% (SD = 16.684) at 3 months. Flt3CreER|Tom/Tom samples exhibited continuous low Ter119- counts, with 38.95% (SD = 8.680) at 1 month, 39.5% (SD = 12.162) at 2 months, and 30.6% (SD = 6.157) at 3 months. For fig. 21C, the average percentages of Ly6G+ cells within the Ter119- population in experimental and control groups is shown. Initially, Ly6G+ cells made up 38.15% (SD = 19.870) of the Ter119- population in Flt3CreER|Tom/DTA mice, but was found to have gradually decreased at 2 months (23.9 ± 6.149) and even further at 3 months (18.467 ± 18.649). In Flt3CreER|Tom/Tom mice, however, there was a high

percentage of Ly6G+ cells at 1 month (50.75 ± 5.869), which significantly dropped to 10.41% (SD = 1.259) at 2 months and stayed there at 3 months (10.8 ± 3.244).

Chapter IX.

Discussion

Incorporating the flow cytometry analysis of both lymphoid and myeloid cell types over the three-month period, there are several conclusions that can be inferred from the data.

MPPs and Myeloid Bias

In both Flt3CreER|Tom/DTA and Flt3CreER|Tom/Tom mice, a similar number of Tomato+ cells was perceived throughout the three-month period (fig. 16A, fig. 21A). This was promising because the consistency of the Tomato+ events between lymphoid and myeloid cell populations confirmed that the presence and detection of Tomato+ cells was not restricted by sample preparation or incorrect flow cytometry set up. However, there was a difference between the percentage of Tomato+ Ter119- cells recorded in experimental and control mice when examining lymphoid cells versus myeloid cells (fig. 16B, fig. 21B). This was unexpected as the proportion of Tomato+ cells that are Ter119- should be fairly consistent between Flt3CreER|Tom/DTA samples and between Flt3CreER|Tom/Tom samples, regardless of whether they were being examined for myeloid or lymphoid cells. However, this could be due to inconsistencies in the RBC lysis-driven removal of erythrocytes between samples, which would result in a greater presence of Ter119-expressing erythrocytes in samples that had not been properly lysed. Focusing on the more relevant cell types, flow cytometry data suggests that the depletion of multipotent progenitors resulted in the gradual reduction of granulocytes compared to a significant depletion observed in control mice (fig. 21C). Additionally, MPP depletion

seems to cause the CD4+ T cell population to initially increase, evident by the difference in CD4+ T cell counts in experimental versus control mice at 1 month (fig. 16C). However, by the second month, CD4+ T cell levels in Flt3CreER|Tom/DTA samples had lowered to those observed in control samples and maintained similar levels at month 3 as well. CD8+ T cell levels, on the other hand, seem to remain relatively unchanged by the targeted eradication of MPPs at 1 month, but appear to become suppressed by month 2 in contrast to the levels observed in control mice (fig. 16D). Though, this observation was not detected at the third month as CD8+ T cells in Flt3CreER|Tom/DTA samples increased to Flt3CreER|Tom/Tom CD8+ T cell numbers. Finally, CD19+ B cells remained largely unchanged in Flt3CreER|Tom/DTA samples, whereas control samples demonstrated continuously increasing levels (fig. 16E).

Overall, these results indicate that the surviving MPPs in experimental samples were able to remedy the effects of MPP depletion and support the continued production of T cells and B cells. As explained previously, CD4 T cells increased in the initial effects of MPP elimination and then returned to levels similar to controls (fig. 16C). Not only is it clear that the diminishment of MPPs caused the Tomato+ T cell population to briefly increase, but the Tomato-positive aspect demonstrates that the tdTomato-labeled surviving MPPs specifically sustained the generation of CD4 T cells. This was also observed in the CD8 T cell population as the surviving Tomato+ MPPs in experimental mice were able to maintain Tomato+ CD8 T cell levels consistent with controls (fig. 16D). Moreover, the results observed in the CD19 B cell population suggest that the surviving MPPs in experimental samples produced an overabundance of B cells, evident by experimental mice having consistently higher numbers than control mice throughout

the three-month period (fig. 16E). All in all, additional research is needed to further understand the influence of MPP depletion on myeloid and lymphoid cells and characterize the changes observed in this project.

References

Bousounis, Pavlos, et al. “Inflammation, Aging and Hematopoiesis: A Complex Relationship.” *Cells*, vol. 10, no. 6, 2021, https://doi.org/10.3390/cells10061386. Accessed 7 September 2023.

Brunetti, Lorenzo, et al. “DNMT3A in Leukemia.” *Cold Spring Harbor Perspectives in Medicine*, vol. 7, no. 2, 2017, https://doi.org/10.1101%2Fcshperspect.a030320. Accessed 10 October 2023.

Challen, Grant A., et al. “Mouse Hematopoietic Stem Cell Identification And Analysis.” *Cytometry*, vol. 75A, no. 1, 2009, pp. 14-24, https://doi.org/10.1002%2Fcyto.a.20674. Accessed 10 September 2023.

Dignum, Tessa, et al. “Multipotent progenitors and hematopoietic stem cells arise independently from hemogenic endothelium in the mouse embryo.” *Cell Reports*, vol. 36, no. 11, 2021, pp. 109675, https://doi.org/10.1016/j.celrep.2021.109675. Accessed 3 December 2023.

Gardner, Ian D. “The Effect of Aging on Susceptibility to Infection.” *Reviews of Infectious Diseases*, vol. 2, no. 5, 1980, pp. 801-810, https://doi.org/10.1093/clinids/2.5.801. Accessed 19 September 2023.

Gazit, Roi, et al. “Fgd5 identifies hematopoietic stem cells in the murine bone marrow.” *Journal of Experimental Medicine*, vol. 211, no. 7, 2014, pp. 1315-1331, https://doi.org/10.1084%2Fjem.20130428. Accessed 23 October 2023.

Genovese, Giulio, et al. “Clonal Hematopoiesis and Blood-Cancer Risk Inferred from Blood DNA Sequence.” *New England Journal of Medicine*, vol. 371, no. 26, 2014, pp. 2477-2487, https://doi.org/10.1056%2FNEJMoa1409405. Accessed 10 November 2023.

Guo, Jun, et al. “Aging and age-related diseases: from molecular mechanisms to interventions and treatments.” *Signal Transduction and Targeted Therapy*, vol. 7, no. 391, 2022, https://doi.org/10.1038/s41392-022-01251-0. Accessed 19 September 2023.

Jaiswal, Siddhartha. “Clonal hematopoiesis and nonhematologic disorders.” *Blood*, vol. 136, no. 14, 2020, pp. 1606-1614, https://doi.org/10.1182%2Fblood.2019000989. Accessed 10 October 2023.

Jaiswal, Siddhartha, and Ebert, Benjamin L. “Clonal hematopoiesis in human aging and disease.” *Science*, vol. 366, no. 6465, 2019, https://doi.org/10.1126%2Fscience.aan4673. Accessed 10 October 2023.

Jaiswal, Siddhartha, et al. “Age-Related Clonal Hematopoiesis Associated with Adverse Outcomes.” *New England Journal of Medicine*, vol. 371, no. 26, 2014, pp. 2488-2498, https://doi.org/10.1056%2FNEJMoa1408617. Accessed 10 October 2023.

Kline, Kline A., and Bowdish, Dawn M.E. “Infection in an aging population.” *Current Opinion in Microbiology*, vol. 29, 2016, pp. 63-67, https://doi.org/10.1016/j.mib.2015.11.003. Accessed 19 September 2023.

Kobayashi, Michihiro, et al. “HSC-independent definitive hematopoietic cells persist into adult life.” *Cell Reports*, vol. 42, no. 3, 2021, pp. 112239, https://doi.org/10.1101/2021.12.02.468909. Accessed 3 December 2023.

Lai, Anne Y., et al. “Heterogeneity of Flt3-Expressing Multipotent Progenitors in Mouse Bone Marrow.” Journal of Immunology, vol. 175, no. 8, 2005, pp. 5016-5023, https://doi.org/10.4049/jimmunol.175.8.5016. Accessed 28 November 2023.

Lee, Jungwoon, et al. “Causes and Mechanisms of Hematopoietic Stem Cell Aging.” *International Journal of Molecular Sciences*, vol. 20, no. 6, 2019, pp. 1272, https://doi.org/10.3390%2Fijms20061272. Accessed 19 September 2023.

Loberg, Matthew A., et al. “Sequentially inducible mouse models reveals that Npm1 mutation causes malignant transformation of Dnmt3a-mutant clonal hematopoiesis.” *Leukemia*, vol. 33, no. 7, 2019, pp. 1635-1649, https://doi.org/10.1038%2Fs41375-018-0368-6. Accessed 10 October 2023.

Luis, Tiago C., et al. “Biological implications of clonal hematopoiesis.” *Experimental Hematology*, vol. 77, 2019, pp. 1-5, https://doi.org/10.1016/j.exphem.2019.08.004. Accessed 7 September 2023.

McKerrell, Thomas, et al. “Leukemia-Associated Somatic Mutations Drive Patterns of Age-Related Clonal Hematopoiesis.” *Cell Reports*, vol. 10, no. 8, 2015, pp. 1239-1245, https://doi.org/10.1016%2Fj.celrep.2015.02.005. Accessed 10 October 2023.

Meija-Ramirez, Eva, and Florian, Maria C. “Understanding intrinsic hematopoietic stem cell aging.” *Haematologica*, vol. 105, no. 1, 2020, pp. 22-37, https://doi.org/10.3324/haematol.2018.211342. Accessed 17 September 2023.

Orkin, Stuart H., and Zon, Leonard I. “Hematopoiesis: An Evolving Paradigm for Stem Cell Biology.” *Cells*, vol. 132, no. 4, 2008, pp. 631-644, https://doi.org/10.1016/j.cell.2008.01.025. Accessed 7 September 2023.

Patel, Sachin H., et al. “Lifelong multilineage contribution by embryonic-born blood progenitors.” *Nature*, vol. 606, no. 7915, 2022, pp. 747-753, https://doi.org/10.1038/s41586-022-04804-z. Accessed 1 September 2023.

Seita, Jun, and Weissman, Irving L. “Hematopoietic Stem Cell: Self-renewal versus Differentiation.” *Wiley Interdisciplinary Reviews: Systems Biology and Medicine*, vol. 2, no. 6, 2010, pp. 640-653, https://doi.org/10.1002/wsbm.86. Accessed 7 September 2023.

Shulsh, Liran I. “Age-related clonal hematopoiesis.” *Blood*, vol. 131, no. 5, 2018, pp. 496-504, https://doi.org/10.1182/blood-2017-07-746453. Accessed 15 September 2023.

Tian, Chen, and Zhang, Yizhuo. “Purification of hematopoietic stem cells from bone marrow.” *Annals of Hematology*, vol. 95, 2016, pp. 543-547, https://doi.org/10.1007/s00277-016-2608-z. Accessed 28 November 2023.

Venugopal, Kartika, et al. “Alterations to DNMT3A in Hematologic Malignancies.” *Cancer Research*, vol. 81, no. 2, 2021, pp. 254-263, https://doi.org/10.1158/0008-5472.CAN-20-3033. Accessed 10 October 2023.

Wilkinson, Adam C., et al. “Long-term ex vivo haematopoietic-stem-cell expansion allows nonconditioned transplantation.” *Nature*, vol. 571, 2019, pp. 117–121, https://doi.org/10.1038/s41586-019-1244-x. Accessed 28 November 2023.

Xie, Shaoping, et al. “Cloning, expression and chromosome locations of the human DNMT3 gene family.” *Gene*, vol. 236, no. 1, 1999, pp. 87-95, https://doi.org/10.1016/s0378-1119(99)00252-8. Accessed 10 October 2023.

Yang, Liubin, et al. “DNMT3A in haematological malignancies.” *Nature Reviews Cancer*, vol. 15, no. 3, 2015, pp. 152-165, https://doi.org/10.1038%2Fnrc3895. Accessed 10 October 2023.

Yokomizo, Tomomasa, and Dzierzak, Elaine. “Three-dimensional cartography of hematopoietic clusters in the vasculature of whole mouse embryos.” *Development*, vol. 137, no. 21, 2010, pp. 3651-3661, https://doi.org/10.1242/dev.051094. Accessed 3 December 2023.

Yokomizo, Tomomasa, et al. “Independent origins of fetal liver hematopoietic stem and progenitor cells.” *Nature*, vol. 609, 2022, pp. 779-784, https://doi.org/10.1038/s41586-022-05203-0. Accessed 15 December 2023.